

# Chapter 7

## Structural Studies of Nucleic Acids



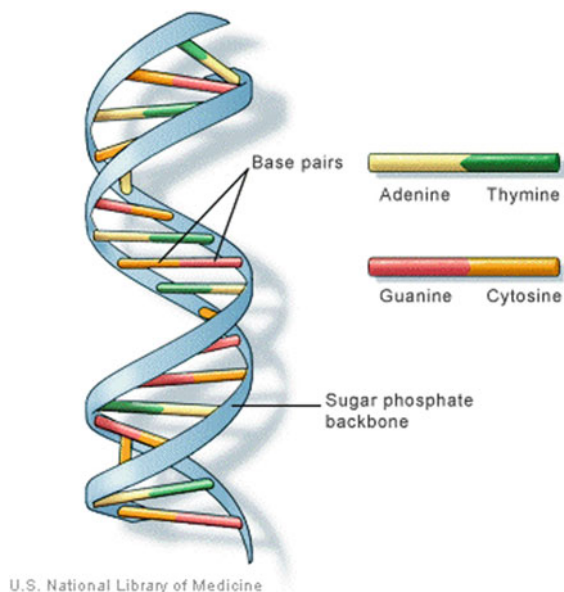
**Abstract** Nucleic acids have a very rich range of structures that are important in many biological contexts. PELDOR or DEER spectroscopy has provided a unique glimpse at the structures that form in solution and guide the response of the cellular machinery.

DNA and RNA nucleic acids have backbones consisting of chains of alternating sugar and phosphate groups linked by ester bonds. A nitrogenous base is attached to each sugar. The bases interact with each other and tend to stabilize DNA in a double helix Fig. 7.1, while RNA has a richer range of structures.

The bases commonly found in DNA are adenine (A), guanine (G), cytosine (C) and thymine (T). RNA is similar, but contains uracil (U) instead of thymine, and the sugar is ribose instead of deoxyribose. Each nitrogenous base can form stable hydrogen bonds with another base to stabilize the three-dimensional structure of the nucleic acid. Thymine pairs with adenine, while guanine pairs with cytosine. In RNA, uracil pairs with adenine.

Nucleic acids are the carriers of the genetic code in biological systems, but also have important regulatory, structural and catalytic roles. Cells modify particular bases, often by methylation, to cause major and minor structural changes that they use to regulate nucleic acid functions. Cells also need to recognize the structural changes in DNA that is damaged, e.g., by radiation or oxidative stress, so that the damage can be repaired or destroyed. Structural information about intact and

**Fig. 7.1** Schematic representation of DNA structure. Courtesy of the National Library of Medicine



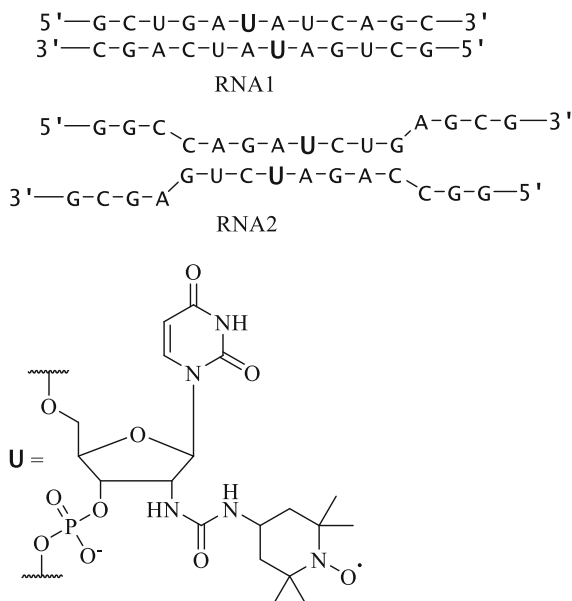
damaged DNA, RNA and their complexes in various biological systems is a primary goal of many physical studies, including PELDOR, in biology.

The success of PELDOR research in this area is a direct result of the effective methods developed for site-directed spin labeling, Sect. 4.3. PELDOR studies of DNA and RNA have investigated several specific biochemical systems. However, this work is only briefly discussed in reviews [1–7] and only in combination with other applications of PELDOR. This Chapter covers the application of PELDOR to DNA and RNA.

## 7.1 Linear Duplexes of Nucleic Acids

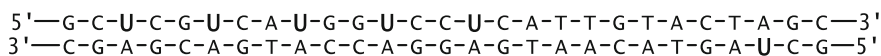
### 7.1.1 Duplex Formation

The structures of 12-bp (base pair) duplex **RNA1**, with all bases paired, and 15-bp duplex **RNA2**, with only eight paired bases at the center and unpaired bases at both ends, were investigated [8]. TEMPO labels **4-19** were attached to the amino groups of 2-amino-ribose in 2'-amino uridine **U** residues via reaction with TEMPO isothiocyanates.



A modulated 3pPELDOR time trace  $V(T)$  was seen in aqueous buffer only for **RNA1**. The distance between spin labels  $r = 3.5 \pm 0.2$  nm was determined by Fourier analysis. The  $V(T)$  for **RNA2** showed only an exponential decay, which indicated a uniform volume distribution of spin labels. This means that no duplexes formed between spin-labeled **RNA2** oligonucleotides at 0.3 mM in aqueous buffer: 0.1 M NaCl, 0.01 M Na-phosphate, 0.1 mM Na<sub>2</sub>EDTA, pH 7.2. Both RNA sequences are palindromic, indicating that the duplex sequence would be identical when read from either end of the duplex. Unfortunately, this also means that intramolecular hairpin structures with only one spin label can form instead of the desired bimolecular duplex. Na-phosphate is a notoriously poor choice of buffer for frozen solutions because it can undergo extreme shifts in pH as it freezes [9].

A series of 27-bp DNA duplexes was studied with spin labels attached at 2'-amino uridine residues in different strands by reaction with TEMPO isocyanate. The DNA duplexes had interspin distances of 9, 12, 15, 18 or 21 bp:



with the spin-labeled nucleotide sites shown in bold [10]. Five different doubly spin-labeled duplexes were synthesized. The spin label pairs with distances ranging from 2.8 to 6.8 nm are shown schematically in Fig. 7.2.

The distance distribution  $F(r)$  of individual duplexes gave distinct peaks at distances corresponding to the expected interspin distances. More interestingly, mixtures of two duplexes have  $F(r)$  that show the distances for both duplexes in the mixture, with amplitudes reflecting the relative concentrations, Fig. 7.3.

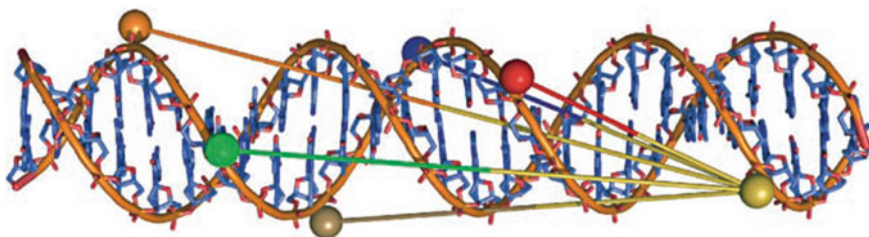


**Fig. 7.2** Molecular model showing the positions of spin label pairs for distance measurements. Reprinted from Ward et al. [10] with permission of Wiley and Sons, copyright 2007

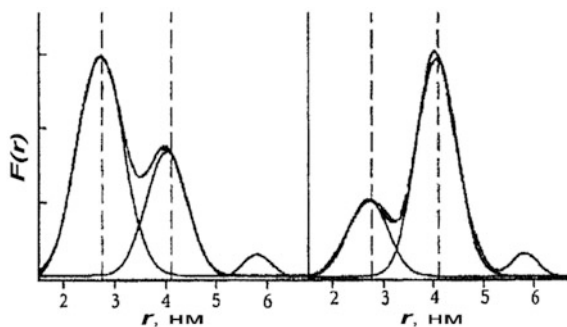
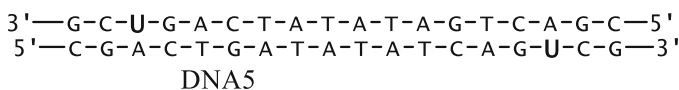
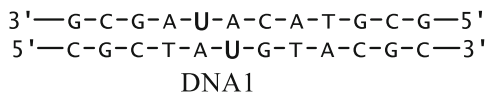


**Fig. 7.3** Mixtures of spin-labeled DNA duplexes:  $F(r)$  are shown for mixtures of labeled DNA duplexes with distances of 2.8 nm and 4.1 nm, **Left**: in a 3/1 ratio; **Right**: in a 1/3 ratio. Reprinted from Ward et al. [10] with permission of Wiley and Sons, copyright 2007

Deconvolution of  $F(r)$  for the mixture using a Gaussian curve for each duplex yields the average distance in each duplex and its concentration in the mixture with good accuracy [10].

### 7.1.2 Duplex Conformation

TPA **4-18** spin labels were introduced via reaction B in Sect. 4.3.3 into 2'-deoxy-uridine dU residues of five different DNA duplexes and distances between the labels were determined using 4pPELDOR [11]. The number of bases between the labels,  $n$ , was different:  $n = 0, 2, 8, 10, 12$ , for **DNA1–DNA5**, respectively. For instance, **DNA1** and **DNA5**, with the spin-labeled dU residues indicated here as **U**, are:



The duplexes were investigated at 35 K in aqueous buffered solutions with 20% ethylene glycol added to form a good glass. The modulation of the PELDOR  $V(T)$  was recorded for all DNA molecules, Fig. 7.4. The modulation period increased as the distance between the spin labels increased. The Fourier spectra in all the cases had the shape of Pake doublets, Fig. 7.5. The features at 7.4 and 14.8 MHz in this doublet correspond to the parallel  $\theta = 0^\circ$  and perpendicular  $\theta = 90^\circ$  orientations of the vector connecting the spin labels relative to the external magnetic field direction. The distance between the labels is  $r = 1.92$  nm from Eqs. 1.1 and 1.2 with the exchange integral  $J = 0$ . The distances for **DNA2–DNA5** were 2.33, 3.47, 4.48, and 5.25 nm, respectively. These distances, with their uncertainties, are in excellent agreement with values from MD simulations for the B-conformation of the duplex helix, Fig. 7.6 [11]. The correlation coefficient for the two sets of data is 0.997, supporting existence of the B-conformation in frozen aqueous solutions [11]. A detailed comparison of PELDOR and FRET [11] measurements on these oligomers demonstrated that these methods complement each other well.

Six RNA duplexes labeled with TPA **4-18** were synthesized and their  $V(T)$  had sufficiently deep modulation to calculate the  $F(r)$  [12]. The distances between spins in the duplexes range from  $1.93 \pm 0.12$  to  $3.87 \pm 0.13$  nm, depending on the number of base pairs between labels. Comparison of these experimental results in RNA [12] with the results just discussed for the same spin label in DNA [11] indicate that distances between labels on different helices are different in DNA and RNA. For example, for labels separated by 10 bp, the distance between them is  $4.48 \pm 0.50$  nm in DNA but  $3.87 \pm 0.13$  nm RNA [12]. The difference is too large to be accounted for by measurement error; but it does correspond to two different nucleic acid conformations: the A-form in RNA and the more-stretched B-form in DNA. The experimental distances are in good agreement with MD simulations: the correlation coefficient was 0.976 [12]. The DNA and RNA duplexes maintain their conformations in frozen aqueous phosphate buffer solutions with ethylene glycol.

### 7.1.3 Labeled Phosphate Groups

TPA **4-18** labels have been attached via a methylene linker to phosphorothioate groups at specific positions along the sugar-phosphate backbone rather than onto the nitrogenous base [13]. Eight interspin distances from 2.56 to 3.88 nm were

**Fig. 7.4** PELDOR time traces  $V_{\text{INTRA}}(T)$  for spin-labeled DNA1-DNA5. Reprinted from Schiemann et al. [11] with permission of American Chemical Society, copyright 2004

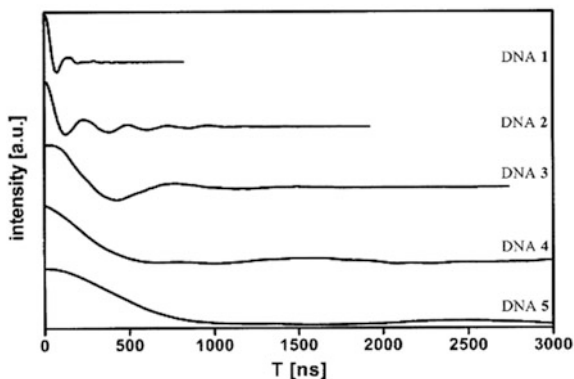


**Fig. 7.5** Fourier spectrum of  $V_{\text{INTRA}}$  for DNA1 showing a broadened Pake pattern. Reprinted from Schiemann et al. [11] with permission of American Chemical Society, copyright 2004

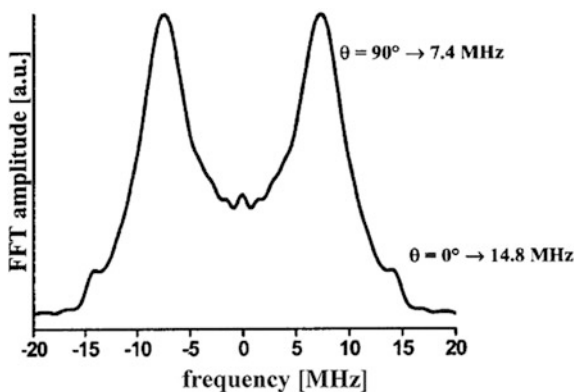
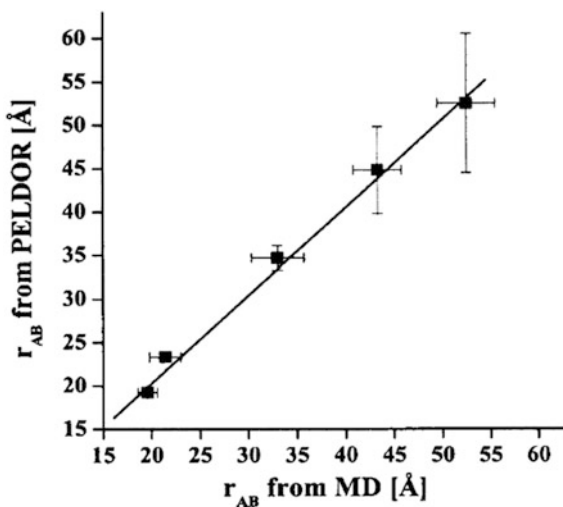


**Fig. 7.6** Correlation of distances  $r_{\text{AB}}$  obtained by PELDOR experiment and MD calculations. Reprinted from Schiemann et al. [11] with permission of American Chemical Society, copyright 2004



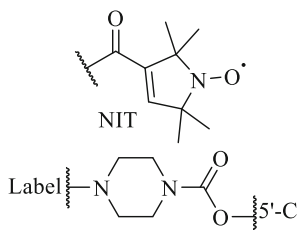
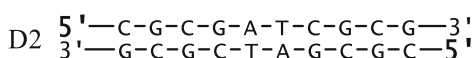
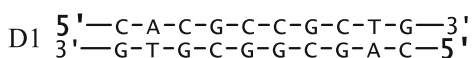
determined in a set of 12-bp DNA duplexes from the maxima of peaks in the PELDOR  $F(r)$ . This method of labeling readily scales to long polynucleotides [13]. An example of a 68-bp DNA fragment with labels on opposite strands 9 nucleotides from one end of the duplex is given. The 2.52 nm distance between spins that is measured by PELDOR for this duplex agreed with the 2.5 nm distance from MD simulations.

The distance from PELDOR was compared with that from NMR, giving an excellent correlation of  $R^2 = 0.98$  [13]. This labeling strategy was proposed for structural studies of DNA and RNA complexes with protein.

A similar investigation introduced spin labels into phosphorothioate groups of RNA [14]. Six sets of interspin distances ranging from 2.5 to 4.72 nm were compared to X-ray structures. A strong correlation between these measurements was found with  $R^2 = 0.97$ . The introduction of the label does not seem to significantly alter the nucleic acid structure.

### 7.1.4 End Labels

It is rather easy to attach a label to the 5' end of a nucleic acid duplex of any length. Larger labels can be accommodated at the end of a duplex than along the side of a duplex. This opens up the use of Trityl **T 4-2** spin labels, with a narrower spectrum and slower relaxation than nitroxyls, for EPR distance measurements. The use of trityl labels was tested in a series of model DNA duplexes **D1**, **D2** end-labeled with either **T** or nitroxyl **NIT** [15]. The spin labels were attached to the 5' end by two different linkers, a short  $-\text{NH}_2-$  and a longer linker known as PIP:

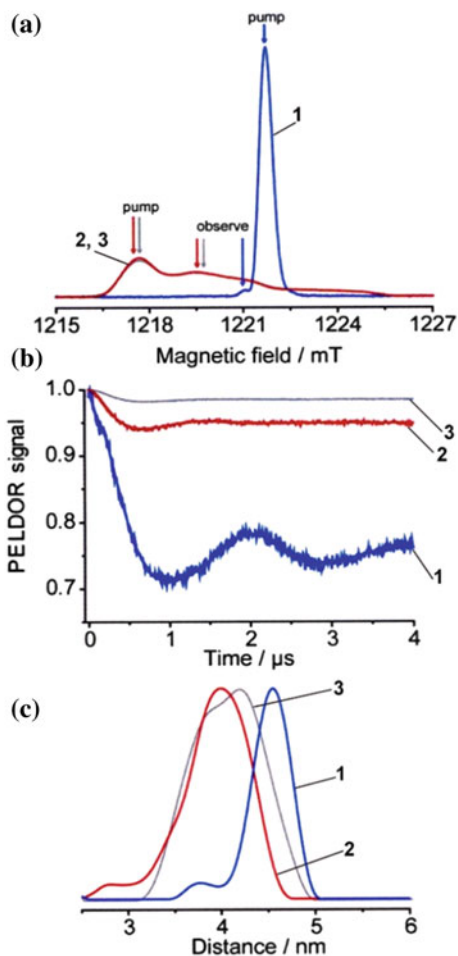


The width  $\Delta$  of the distance distributions, obtained by Q-band 4pPELDOR at 80 K, strongly depends on the type of label. Replacement of both **NIT** by **T** in the same duplex sharpens the distance distribution, Table 7.1. Duplexes with one **NIT** and one **T**, sometimes called orthogonal labeling, have a less pronounced sharpening, but a significant gain in sensitivity due to more efficient pumping of the narrow EPR spectrum of **T**, Fig. 7.7. The width of the distance distribution  $\Delta$  with

**Table 7.1** Distances  $r$  and distance distribution widths  $\Delta$  in DNA duplexes **D1**, **D2** labeled by trityls **T** and nitroxy **NIT** [15]

DNA Complex	Distance, $r$ (nm)	$\frac{1}{2} \Delta$ (nm)*
<b>D1-PIP-T/T</b>	4.54	0.20
<b>D1-PIP-NIT/NIT</b>	4.24	0.62
<b>D1-NH-NIT/NIT</b>	3.91	0.37
<b>D2-NH-T/T</b>	4.49	0.25
<b>D2-PIP-T/T</b>	4.50	0.18
<b>D2-NH-NIT/NIT</b>	4.05	0.36

**Fig. 7.7** **a** Echo-detected EPR spectra of duplexes: 1: **D2-NH-T/T**, 2: **D1-NH-NIT/NIT** and 3: **D2-NH-NIT/NIT**, spectral positions of pump and observe pulses are indicated for each duplex; **b** PELDOR  $V(T)$  for each duplex after removal of relaxation background; **c**  $F(r)$  obtained for each duplex. Reproduced from Shevelev et al. [15] with permission of American Chemical Society, copyright 2015



**NIT/NIT** labels does depend on the linker: the shorter amine-based linker improves  $\Delta$  by a factor of two. On the other hand, the linker length has no effect on  $\Delta$  with **T/T** labels. MD calculations indicate greater conformational disorder of the **NIT**



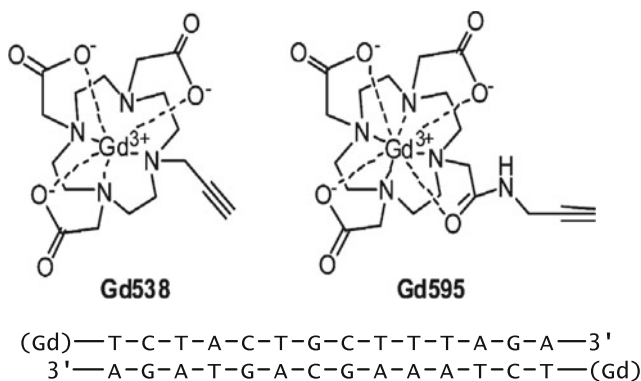
labels compared to **T**, thus rationalizing the experimentally observed trends. In fact, the MD calculations show that hydrophobic areas on the **T** label cap the stack of bases at the end of the duplex [15].

Labeling with **T** gives narrower spin-spin distance distributions and potentially more precise distances between labeling sites than does more traditional nitroxyl labels. However, the distances in **NIT/NIT** pairs with the short linker are actually nearer to the length of ten-bp B-helix DNA. The  $\sim 1$  nm diameter of **T**-labels must be considered in distance measurements [15].

The ten-bp **D1-PIP-T/T** and **D2-PIP-T/T** duplexes were measured by DQC at 310 K and at 80 K by PELDOR, giving the same distance,  $\sim 4.6$  nm [16]. The DNA was immobilized on NucleosilDMA sorbent, which prevented movement of the **T** label.

Gd(III) [17–19] or Cu(II) [20] complexes have been recently suggested for use as labels, Sects. 4.2 and 4.4. These labels are typically characterized by a rather complex EPR spectrum in polyoriented systems. However, for Gd(III), the  $-1/2 \rightarrow +1/2$  transition, dominates the spectrum at Ka-band for temperatures of  $\sim 10$  K and is used in PELDOR experiments.

The structure of a 14-bp duplex was investigated using Gd(III) complexes **Gd538** and **Gd595** as labels incorporated at the terminal thymidine molecules using “click chemistry” [19]. The 4pPELDOR measurements found a distance of  $5.9 \pm 1.2$  nm between the ions in these DNA duplexes, while the width of the distribution was  $\sim 2$  nm. The use of Gd(III) labels might increase the range of PELDOR-measured distances to  $\sim 10$  nm [19], which is significant for some complex biomolecules. The relatively large distance, 1.2–1.5 nm, between the ions and the position of attachment to the macromolecule results in a wide distance distribution and a decrease in the measurement accuracy due to the mobility of these labels. This is an obvious drawback of these labels in comparison to nitroxyl labels. A number of features of the PELDOR analysis methods for Gd(III) and Cu(II) have been thoroughly examined [19, 20].

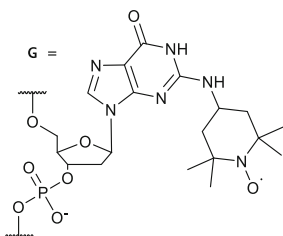
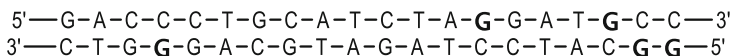


### 7.1.5 Conformational Changes

The studies just described show that spin labeling of linear DNA and RNA duplexes allow a rather consistent determination, to  $\sim 1\%$ , of the distance between the spin-labeled nucleotides.

The strong correlation between PELDOR and MD results is very significant. The MD simulations are typically carried out for room temperatures and aqueous solutions, while the PELDOR measurements were made with rapidly-frozen glassy solutions. The conformations of DNA and RNA molecules at room temperature seem to persist even through flash freezing of the solutions. This suggests that PELDOR will give relevant structural information for nucleic acids in other environments, with novel interactions, and during reactions.

Changes in the distance between nucleotides during the transition from the B- to the A-form of DNA have been studied using PELDOR [21]. A series of spin-labeled DNA duplexes were investigated:



where the sites of spin labels are shown in bold.

The 4-amino-TEMPO **4-19** label was attached to the N2 atom of specific guanine residues. Labels were attached either to the same helix at positions denoted (**4;19**) and (**4;20**), or to different helices at positions denoted (**4;14'**) or (**4;18'**). The transition between the B- and A-forms of DNA occurs in polar media. PELDOR measurements were made at 60–70 K in aqueous buffer with 10 vol. % glycerol added as a cryoprotectant [21].

Addition of trifluoroethanol, TFE, stimulated the B  $\rightarrow$  A transition. The distance spectrum changed with the volumetric content of TFE, Fig. 7.8. The longer B-form converts into the more compact A-form as the TFE concentration exceeds 70%. The measured interspin distances in the A- and B-forms agree well with distances between the oxygen atoms of the  $>\text{NO}$  groups of the spin labels from MD simulations, Table 7.2 [21].

The ability of PELDOR to determine distances in the nanometer range is considerably better than that of any other method, such as CW EPR or circular

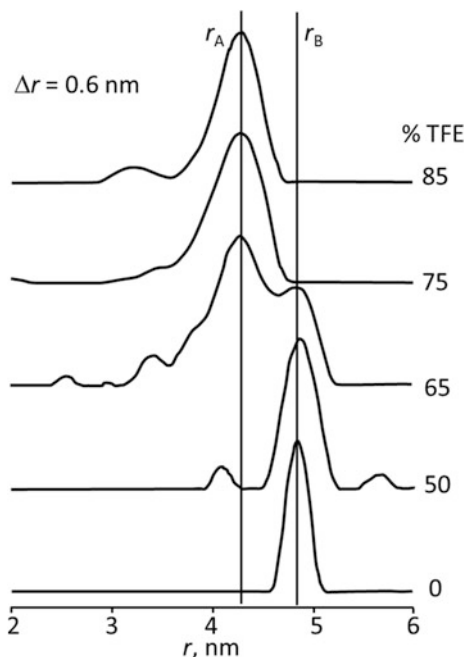


**Fig. 7.8** The measured  $F(r)$  as TFE is added to an aqueous solution of (4;18')-labeled DNA duplex. Reprinted from Sicoli et al. [21] with permission of Wiley and Sons, copyright 2008

**Table 7.2** Experimental and calculated distances in nm between the spin labels for the A- and B-forms of DNA [21]

DNA duplex	PELDOR distance	Calculated O–O distance, B-form	PELDOR distance	A-form, calculated O–O distance
(4;20)	$5.6 \pm 0.2$	$5.6 \pm 0.3$	$4.8 \pm 0.2$	$4.5 \pm 0.4$
(4;19)	$5.1 \pm 0.2$	$5.1 \pm 0.3$	$4.6 \pm 0.3$	$4.4 \pm 0.4$
(4;18')	$4.9 \pm 0.2$	$4.8 \pm 0.4$	$4.3 \pm 0.3$	$4.2 \pm 0.4$
(4;14')	$3.2 \pm 0.2$	$3.6 \pm 0.3$	$2.8 \pm 0.3$	$3.3 \pm 0.3$

dichroism [21]. This enabled the investigation of the transitions between the A- and B-forms of RNA and DNA in various molecular environments and polarity.

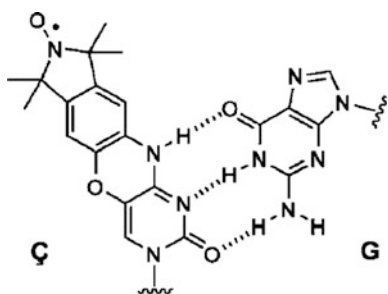
The structure of the nucleic acid can also be altered by the spin label. MD simulations show that a TPA 4-18 spin label in the major groove of DNA or RNA changes the mutual orientation of the base pairs in the molecule [22]. This effect is less significant for labels located in the minor groove. Nonetheless, conformational changes do occur when DNA or RNA is labeled and should be taken into account when interpreting PELDOR results and when planning PELDOR experiments. The

impact of the label was shown in four hybrid DNA/RNA-duplexes. Distances between spin labels have been measured with TPA spin labels attached to the nitrogenous bases so that they were oriented towards either the major or the minor groove of the duplex. This allowed selection of the A- and B-forms of the hybrid [23].

## 7.2 Orientation and Dynamic Properties of DNA

### 7.2.1 Orientation Selection

The distances between spin labels, as well as their mutual orientation, can be determined from orientation selective measurements [24–27]. A special rigid spin label **Ç 4-20** was developed for DNA studies [28]. This label is based on cytosine, and is rigidly oriented and fixed in the DNA duplex by hydrogen bonds with cytosine's complementary base guanine:



The label is coplanar with the guanine and is parallel to the other paired bases and perpendicular to the DNA helix axis, Fig. 7.9 *Left*. The angle between the vector  $r$  connecting the labels and the normal to the plane of each label is the same. This makes it possible to determine the angle  $\beta$  between  $r$  and the helix axis from the PELDOR  $V(T)$  measured with different combinations of  $\omega_A$  and  $\omega_B$ . A detailed description of this analysis and the experimental results are provided in [27]. The  $V(T)$  were measured at X-band for  $\Delta\omega_{AB}/2\pi$  in 10 MHz steps from 40 to 90 MHz. The position of the second label was scanned from  $N3$  to  $N14$ , Fig. 7.9 *Left*. The angle  $\beta$  varied with the position of the label in the DNA, Fig. 7.9 *Right*. The  $\beta$  angle for an idealized DNA duplex corresponds well to the experimental results [27].

Several new labels are suggested for DNA investigations, Fig. 7.10, with differing rigidity when incorporated in DNA oligonucleotides [29].  $^{\text{ExtIm}}\text{U}$  is the first conformally-unambiguous spin label for nucleic acids; the nitroxyl N–O bond is coaxial with the three single bonds attaching the otherwise rigid isoindoline-based spin label to a uracil base. This label has very high rotational mobility around these single bonds in duplex DNA relative to the structurally similar spin label  $^{\text{Im}}\text{U}$ , whose rotation is restricted by an intramolecular hydrogen bond. These labels were

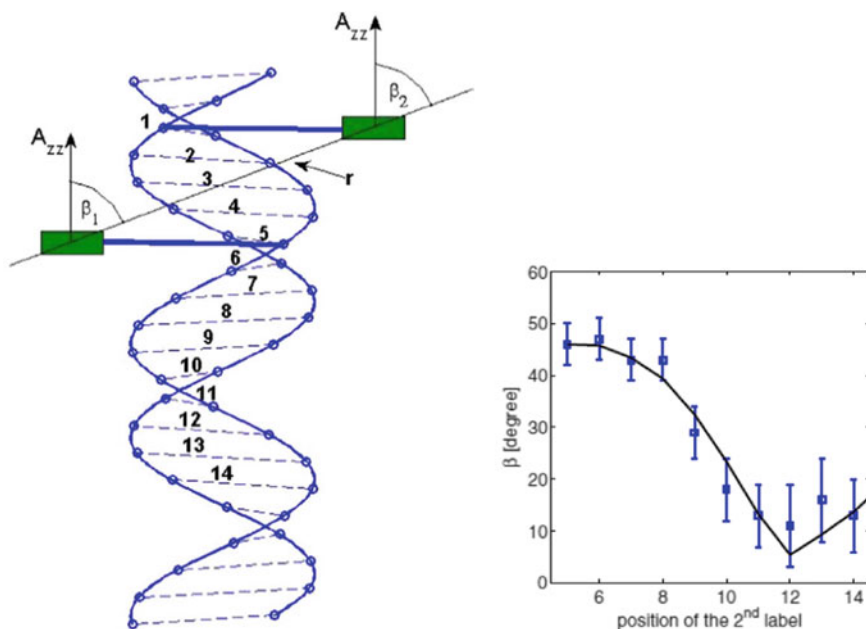


**Fig. 7.9** *Left:* Orientation of spin labels in the DNA structure, spin labels are attached here to the base pairs numbered 1 and 5; the principal axis of hyperfine interaction tensor  $A_{zz}$  is normal to the label plane so the  $\beta_1$  and  $\beta_2$  angles coincide; *Right:* Experimental and calculated dependence of  $\beta = \beta_1 = \beta_2$  on the position of second label. Reprinted from Marko et al. [26] with permission of American Physical Society, copyright 2010

used in two doubly-labeled, 14-bp duplex constructs with either seven- or ten-base pairs between the labels in **DNA(1,9)** and **DNA(1,12)**, respectively [29].

PELDOR distance measurements between pairs of  $\text{ImU}$ ,  $\text{OxU}$ , and  $\text{ExImU}$  in duplex DNA showed strong orientation selection with  $\text{ImU}$  pairs, with  $V(T)$  depending on the location of  $\omega_A$  and  $\omega_B$  in the EPR spectrum. The orientation selection was moderate for  $\text{OxU}$ , and absent for  $\text{ExImU}$ . Thus, precise distances can be extracted from  $\text{ExImU}$  pairs from just a single measurement without having to take orientation selection into account. Interspin distances were obtained at X-band by Tikhonov regularization from sums of  $V(T)$  with  $\Delta\omega_{AB}/2\pi$  from 40 to 85 MHz [29]. The experimental distances for **DNA(1,9)** and **DNA(1,12)** constructs are: 3.43 and 3.41 nm between  $\text{ImU}$  labels; 3.32 and 3.41 nm for  $\text{OxU}$ ; and 4.01 and 3.58 nm for  $\text{ExImU}$ , respectively, in good agreement with calculated models [29].

The first comparative PELDOR study at 263 and 94 GHz examined a model 20-bp RNA duplex system with the rigid **C** label in positions 6 and 16 [30]. There was considerable modulation depth and significant orientation selection at 263 GHz, particularly in the  $g_x - g_y$  plane of the nitroxyl. The difficulties, as well

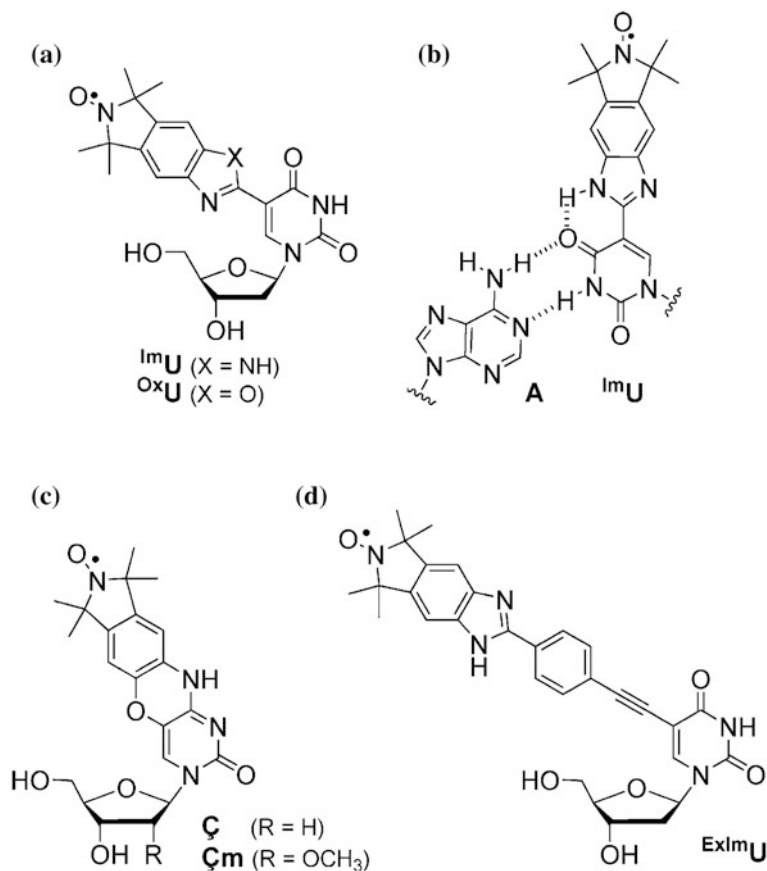


**Fig. 7.10** Spin-labeled nucleosides: **a** isindoline-derived spin labels  $1mU$  and  $oxU$ , **b** base pairing of  $1mU$  with  $A$ , showing the intramolecular hydrogen bond that restricts rotation around the bond connecting the nitroxyl to the base, **c** the rigid spin labels  $C$  and  $Cm$ , **d** the extended benzimidazole spin label  $Ex1mU$ . Reprinted from Gophane et al. [29] with permission of Wiley and Sons, copyright 2007

as the advantages, encountered at such ultrahigh frequencies were noted. There are significant, new possibilities for investigating the orientation of spin labels in structures that are more complex than simple linear single- or double-stranded nucleic acids.

## 7.2.2 Nucleic Acid Dynamics

The dynamic properties of nucleic acids are significant for understanding the kinetics and the mechanisms of cellular processes, e.g., replication and

transcription, in which proteins twist and bend the DNA. Several urgent problems in modern biophysics center on the molecular dynamics of nucleic acids. It was believed, in the early theoretical and experimental research, that the dynamic properties of DNA duplexes could be described by the elastic cylinder model [31]. However, modern physical studies of the mobility of DNA helices [32–34] suggest at least three types of possible motions, including: (A) elongation—the helical pitch changes without any change in diameter; (B) unwinding—the diameter and length change but the pitch does not; and (C) bending—the helix bends without changes in radius or pitch.

It is repeatedly found that the  $F(r)$  obtained from PELDOR measurements on rapidly-frozen glasses, corresponds quite well to the spectrum of conformations that modern MD methods predict in room-temperature liquids. This means that PELDOR can provide a snapshot of the range of dynamics in a molecular system.

These features of PELDOR were used to distinguish between the A, B and C mechanisms in a study of the conformational flexibility of doubly spin-labeled 20-bp DNA [35]. The rigid  $\zeta$  spin label was used and paired labels were attached to 10 model duplexes with one label at one end of the duplex, and the other label was stepped one full turn down the helix. PELDOR measurements were made at X-band,  $\omega_A/2\pi \sim 9$  GHz, and at G-band,  $\sim 180$  GHz. The  $V(T)$  and their dependence on  $\Delta\omega_{AB}$  were measured for all the duplexes. The width  $\Delta = \langle\Delta R^2\rangle^{1/2}$  of the distance distribution, Fig. 7.11a, was determined by averaging the orientation selectivity data [25]. This procedure eliminates correlations between label orientations from the measured distances. In addition, orientation selection measurements were made for all spin pairs [24–26]. The  $V(T)$ , the linewidth of  $F(r)$ , and the mutual orientation of the labels were simulated for the motional model.

The relationship between the width of  $F(r)$  and the position of a label was used to interpret the experimental data, Fig. 7.11b. Only the unwinding model B fit the data. The exact twisting and stretching of the helix in this model can be determined from the orientation selection data obtained in the course of the experiments at G-band. The angle between the N–O bonds of labels one turn apart varied by  $\pm 22^\circ$ . As mentioned in [35], the results completely agree with the model of cooperating fluctuations, the so-called “respiratory” model of DNA duplex motion, where the pitch of a helix remains constant, but the helix radius and the length of the DNA molecule vary in a correlated manner. According to the PELDOR data, the helix radius changes by 11% while the DNA length changes by  $\pm 6\%$ .

These PELDOR results correlate with the small angle X-ray scattering data (SAXS) [34] and with fluorescent microscopy results [32] for short DNA oligomers. The wide variety of experimental approaches used in this work [35]: the unique set of spin-labeled DNA, studies of the orientation selection, measurements at various frequency ranges; revealed the full potential of PELDOR not just for structural studies, but for thorough studies of macromolecular dynamics as well.

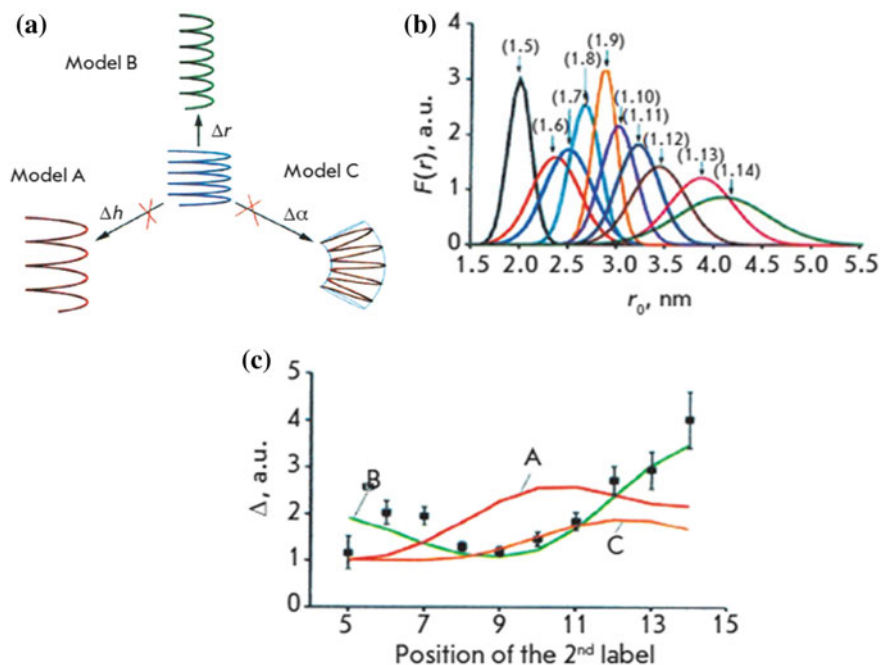


**Fig. 7.11** **a** Three models of motion in duplex DNA (see text); **b**  $F(r)$  from X-band PELDOR data using a Gaussian approximation for  $F(r)$ , with orientation selection for  $\zeta$  spin labels pairs; **c** experimental dependence of the width,  $\Delta = \langle \Delta R^2 \rangle^{1/2}$ , on the distances between the labels and the theoretical simulations for mobility models A, B, and C; the minimal  $\Delta$  value corresponds to the distance between 1 and 9 labels of DNA. Reprinted from Marko et al. [35] with permission of American Chemical Society, copyright 2011

### 7.3 Nonlinear Duplexes and Tertiary Structures

The structure of DNA and RNA is not restricted to a linear helix, but can be much more complex, similar to the tertiary structure of biopolymers. Relatively long single-stranded RNA can form duplexes between their complementary segments, while non-complementary segments form rings, hairpins, and loops, which contain several nucleotides. The distances between specific nucleotides in these secondary structures can differ dramatically from those between nucleotides in ordinary helices.

Distances between TEMPO 4-19 labels attached to the  $-\text{NH}_2$  groups of specific guanine, adenine, or cytosine bases within a RNA hairpin structure 20 nucleotides in length have been measured, Fig. 7.12a [36]. The labels were positioned ten bases apart in a sequence that can fold into a hairpin structure or a duplex if a complementary strand was present. In a duplex, the labels are always 10-bp apart and PELDOR  $V(T)$  give the same distance of 3.1 nm expected for A-form RNA,



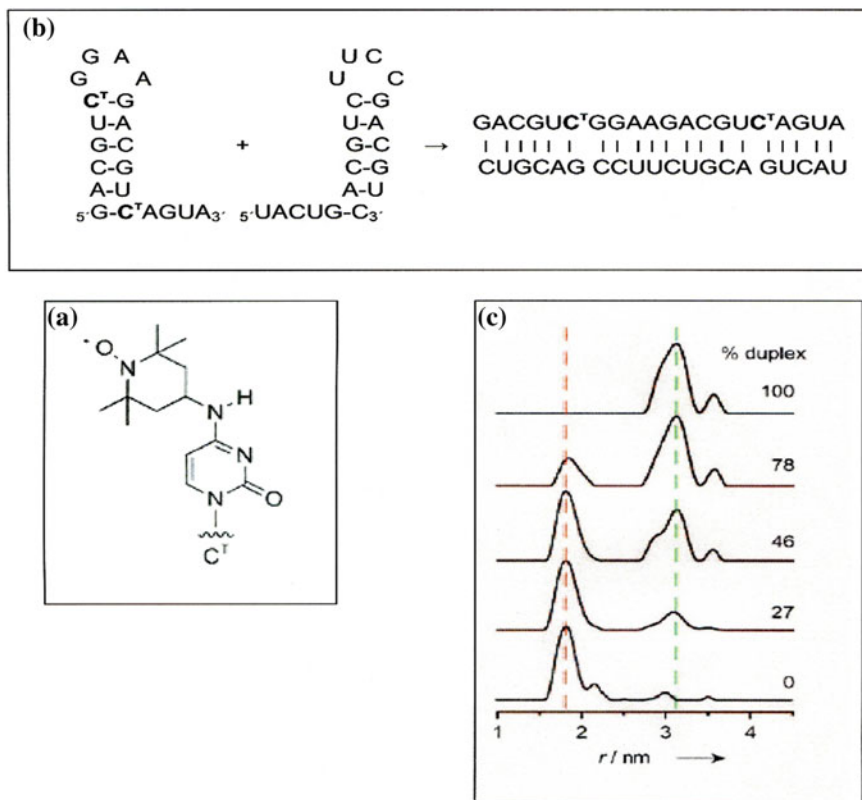


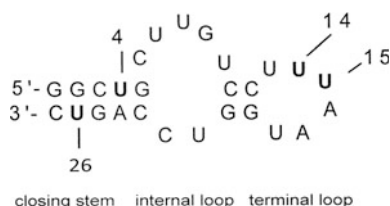
**Fig. 7.12** RNA hairpin investigation: **a** structure of the spin label; **b** formation of a RNA duplex from two hairpins, the hairpin on the left is spin labeled while the other hairpin is complementary but unlabeled, when mixed, the two complementary hairpins can form a duplex; **c** PELDOR distance spectra in the mixtures as the unlabeled, complementary hairpin is titrated into a solution of the labeled hairpin, the distance spectra show the change in relative amount of the RNA duplex. Reproduced from Sicoli et al. [36] with permission of John Wiley and Sons, copyright 2010

regardless of the labeled nucleotide type or the position of the label pair within the RNA duplex.

In this RNA hairpin structure of 20 nucleotides, six complementary nucleotides form a double helix as the hairpin stem, four nucleotides form the loop, and the remaining nucleotides are in a single strand. A duplex with labels only in one strand was formed after a completely complementary RNA molecule without spin labels had been added to the system, Fig. 7.12b. Samples containing different amounts of the labeled RNA and its unlabeled complementary RNA were measured by PELDOR. The distance spectrum obtained in these experiments, Fig. 7.12c, indicates that in frozen buffer solutions, spin-labeled hairpins with 1.8 nm between labels are present, along with duplexes having 3.1 nm between labels.

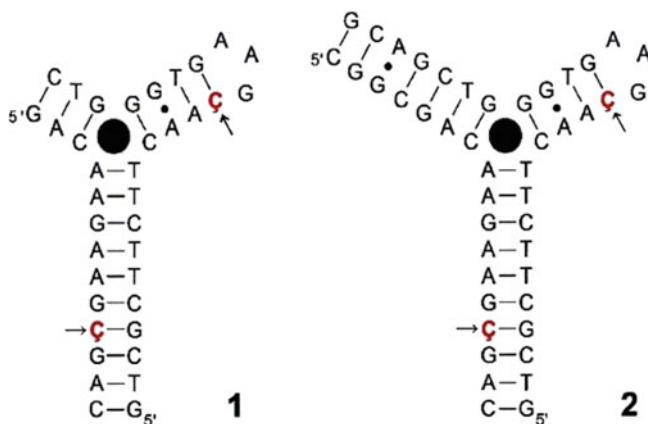
Single RNA strands can form more complex structures, such as rings, or semi-rings, in conjunction with hairpins. These structural elements may respond to certain molecules; they are known as RNA riboswitches and play a crucial role in regulating transfer of genetic information in cells.

Artificially-synthesized RNA riboswitches consisting of 27 nucleotides, that accept neomycin, have been investigated using PELDOR [37]:



TPA **4-18** spin labels were introduced into the bolded uracil residues and the interspin distances between positions 4–14, 4–15, 14–26, 15–26 were determined. An attempt was made to determine the conformational changes in this riboswitch during formation of a neomycin complex [37]. It was found, however, that the distance between the spin-labeled uridine bases were virtually the same in this complex as in the neomycin-free riboswitch. This result suggests that the structure has good conformational stability [37].

The rigid **C 4-20** label was an ideal probe for PELDOR studies on the cocaine aptamer, which is a DNA three-way junction that binds cocaine at its helical junction [38]:



Here two aptamers were studied. Both have the same sequence and are labeled at the same positions, the difference is a longer side helix for aptamer **2**. The filled black circle represents the cocaine ligand. The positions labeled with **C** are marked by arrows.

The conformation and overall flexibility of the aptamer in the presence and absence of cocaine was studied at X- and Q-bands [38]. The C label was incorporated pairwise into two helices of the aptamer. PELDOR orientation selection experiments determined the mutual orientation and the distances between pairs of labels. The cocaine-bound and non-bound states differ in their conformational flexibility, which is lower with cocaine bound. There were only small changes in the width and mean value  $\Delta r = 0.3$  nm of  $F(r)$  upon cocaine binding. A detailed simulation of  $V(T)$  revealed considerable conformational flexibility in the helical junction, even after binding to cocaine.

$Mg^{2+}$  ions had a major effect on the structure of the “hammerhead ribozyme,” HHRz [39]. The distance spectrum for TEMPO 4-19 spin labels incorporated in two stems of the HHRz structure showed that the addition of  $Mg^{2+}$  ions stabilized a tightly-folded structure with the labeled stems quite close  $\sim 2.4$  nm. Without  $Mg^{2+}$  ions or with mutations in other parts of the ribozyme, no ordered structure was observed. It is noteworthy that  $Mg^{2+}$  ions are required for the catalytic activity of this HHRz.

Changes in distances between spin labels that are due to conformational transformations were also seen by PELDOR in other, more complicated RNA and DNA molecules having a range of tertiary structures, see, e.g., [40, 41]. This important area in structural biophysics is ripe for innovative PELDOR studies.

## 7.4 PELDOR Inside Cells

In-cell studies are vital to determine the effect of the intracellular environment and conditions, e.g., viscosity, molecular crowding, the activity of water, interactions with other macromolecules, etc., on the structure of nucleic acids. Such information could be found by PELDOR distances measurements on macromolecules or complexes that contain more than one intrinsic spin or on doubly spin-labeled nucleic acids or proteins introduced into cells.

Sample preparation for EPR studies of doubly spin-labeled nucleic acids or proteins introduced into whole cells is a rather complicated procedure [42–45]. The major approach is the injection method where a large specialized cell, having a diameter about 1 mm, is injected with a solution containing the spin-labeled macromolecule without destroying the cell. This needs to be repeated dozens of times. There is special equipment for microinjection: a glass micropipette with the needle of 0.5–5  $\mu\text{m}$  mounted on a pneumatic or oil-driven injection device is used under a microscope. A detailed description of sample preparation by microinjection can be found in [46]. Although this approach allows the study of a much wider range of nucleic acids and proteins that does the intrinsic radical approach, there can be questions concerning how well the cells, typically oocytes, represent normal physiology of typical cells; how well the injected macromolecules are transported into the proper intracellular compartments; and how much the injected material perturbs the physiological state of the cell.

The main obstacle in conducting in-cell PELDOR experiments is the short half-life of nitroxyl spin labels in the intracellular environment. They are readily reduced by reducing agents, such as small molecules or enzymes, which decrease the EPR signal and convert doubly-labeled molecules into mono-labeled molecules.

A detailed investigation of the decay kinetics of spin labels in cells is given in [47]. The five-member ring, similar to SAT **4-15**, and the six-member ring TOAC **4-22** nitroxyl radicals were studied in *Xenopus laevis* oocyte extracts. The nitroxyl radical stability primarily depended on the size of the heterocyclic ring. The half-life for the five-membered ring nitroxyl is 150 min but for TOAC is 0.7 min. A kinetic analysis of the nitroxyl reduction in cell revealed an enzyme-mediated reaction [47]. These findings in oocyte extracts are important for the selection of the nitroxyl label for in-cell experiments, but results may be different for other cell types, nitroxyl derivatives and conditions. TPA **4-18** is reduced in oocyte extracts about four-fold faster than when it is attached to RNA or DNA [48].

Cells need to be incubated about 1 h at physiological temperatures after microinjection [49], making signal-to-noise an important issue for any in-cell PELDOR measurements. The incubated cells are usually shock-frozen in liquid nitrogen prior to PELDOR experiments made at cryogenic temperatures, but loss of doubly-labeled molecules during incubation is a major concern. A detailed protocol for PELDOR measurements in cells can be found in [46].

### 7.4.1 Ubiquitin

The first in-cell PELDOR experiment was reported in 2010 [49]. Two doubly-labeled constructs of human ubiquitin, a small regulatory protein, were made with five-membered-ring spin labels and injected into *X. laevis* oocytes. PELDOR from the two constructs found distances of 3.14 and 2.60 nm in the oocytes, while the in vitro values were 3.11 and 2.65 nm, respectively. The width of the distribution function  $F(r)$  increased in the oocytes after a 1 h incubation at 18 °C. This broadening was attributed to some intracellular events but not to changes in the ubiquitin conformation [49]. Ubiquitin has also been studied using Gd(III) labels, see Sect. 7.4.4.

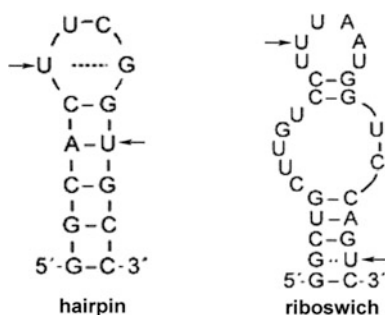
### 7.4.2 Nucleic Acids

PELDOR measurements were made for 12-bp double-labeled DNA in vitro and in cells [48]. The PELDOR  $V(T)$  of in-cell DNA have a somewhat different pattern of oscillation than in vitro. The  $V(T)$  in vitro can be fitted by  $F(r)$  with a single Gaussian peak at 2.1 nm and a width of 0.14 nm, while the in-cell  $V(T)$  requires two Gaussian peaks in their  $F(r)$ . The shorter distance matches the in vitro measurement, indicating that the duplex structure is undisturbed in cells. The longer

distance of 3.7 nm has a very broad width of 2 nm and may arise from the stacking of DNA molecules in cells. End-to-end stacking of 6- to 20-bp nucleic acid duplexes and ordering into semirigid rod-shaped structures is well known [50, 51].

Although in-cell reduction of nitroxyl labels attached to DNA occurs at the same rate as when attached to RNAs, the PELDOR modulation depth for DNA was deeper. This increase in modulation depth was ascribed to dipolar interactions of more than two coupled spins, which could occur with end-to-end stacking of the duplexes. This explanation is further supported by the background  $V_{\text{INTER}}$  which shows a one-dimensional spin distribution with  $d = 1$  Eq. 1.19 as expected for linear stacking of the DNA [48].

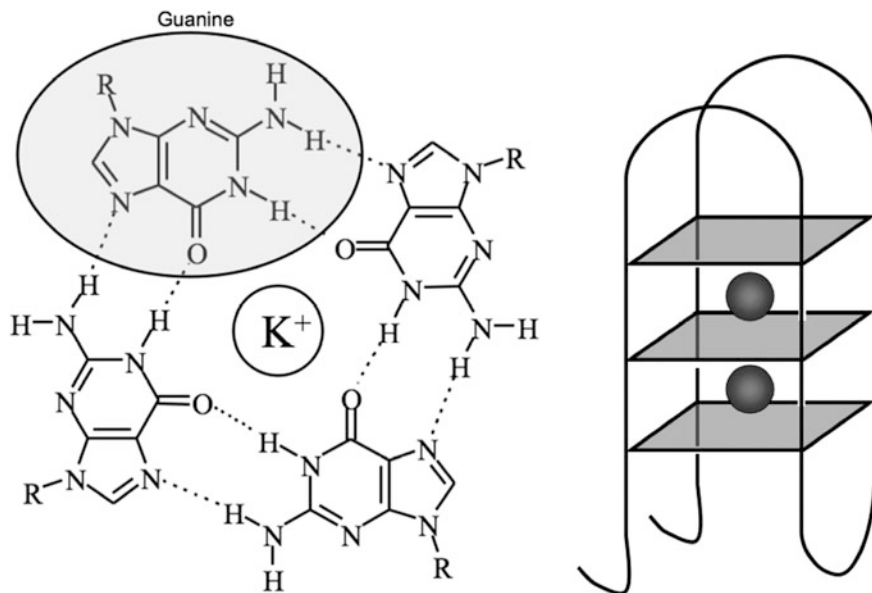
The 14-bp cUUCGg tetraloop hairpin RNA and the 27-bp neomycin-sensing riboswitch were then studied in *X. laevis* oocytes and compared with in vitro PELDOR measurements [48] and with structures of the unlabeled RNA [52, 53].



TPA **4-18** spin labeling at positions shown by arrows took about 50 min. In vitro PELDOR experiments were carried out in intraoocyte buffer. Distances of 1.8 nm for the tetraloop RNA hairpin and 3.4 nm for the neomycin riboswitch were obtained from the in vitro  $V(T)$ . The widths of the  $F(r)$  were 0.27 nm for the hairpin and 0.7 nm for the riboswitch. Practically identical PELDOR results were obtained for both RNAs after 10 and 70 min of incubation. The fact that the distances measured in the in vitro and in-cell experiments were the same implies that the 14-mer hairpin RNA and the 27-mer riboswitch have stable global structures.

### 7.4.3 G-Quadruplexes

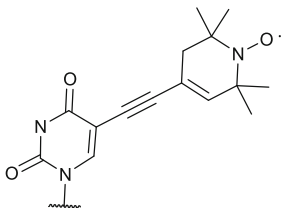
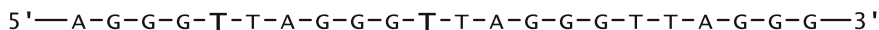
DNA sequences with a high degree of polymorphism are of particular interest for in cell PELDOR measurements because PELDOR can identify different conformations of the DNA constructs. One such important structure is the human telomeric G-quadruplex. The G-quadruplexes are tertiary structures formed by nucleic acids with sequences rich in guanine. Four guanine bases can associate to form a square planar structure, a tetrad, and two or more of these tetrads can stack on top of each other to form a G-quadruplex. The structure is stabilized by a cation, especially  $K^+$ ,



**Fig. 7.13** Schematic outline of the structure of a G-quadruplex *left*: a G-tetrad; *right*: intramolecular loops of nucleic acids linking G-tetrads are shown

sitting in the central channel between each pair of tetrads, Fig. 7.13 [54]. The quadruplex, in response to subtle changes in environmental conditions, is known to adopt drastically different conformations. In particular, its conformation and the mixture of conformations depends upon its counterions,  $K^+$  versus  $Na^+$  and on the DNA sequence around the quadruplex.

The human telomeric quadruplex was studied in buffer with  $K^+$  ions [55]. The conformation in this case is known from NMR and X-ray analysis, Fig. 7.14 [56–58]. In the PELDOR experiments, the DNA sequence  $d[A(GGGTTA)_3GGG]$  was labeled by TEMPA **4-17** in positions 5 and 11, as indicated by a bold **T**:



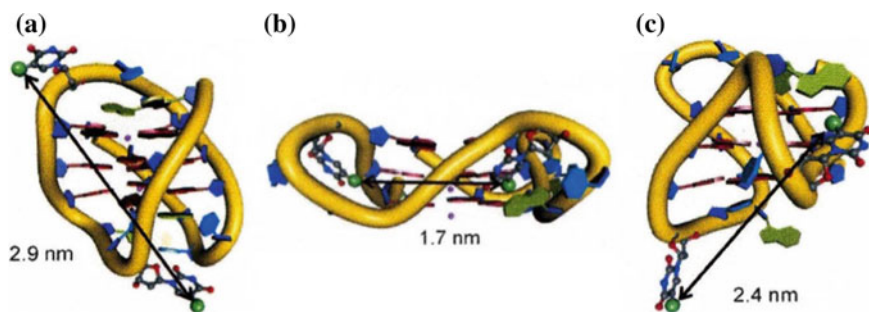


**Fig. 7.14** G-quadruplex topologies based on X-ray and NMR structures: **a** the antiparallel basket quadruplex in the presence of  $\text{Na}^+$  ions [56], **b** the parallel propeller form in the presence of  $\text{K}^+$  ions [57], **c** NMR structure of a hybrid 3 + 1 quadruplex of a slightly modified sequence in  $\text{K}^+$  ions [58]

**Table 7.3** Structural data for G-quadruplex conformations [55, 59]

Conditions	PELDOR experiment (nm)		PDB based calculations (nm)	
	Propeller	Basket	Propeller	Basket
Buffer $\text{K}^+$	$1.8 \pm 0.2$ $\Delta \leq 1.0$	$3.0 \pm 0.1$ $\Delta \leq 1.0$	1.7	2.9
Cells	$2.0 \pm 0.1$ $\Delta = 0.7$	$2.9 \pm 0.1$ $\Delta = 0.7$		

Tikhonov regularization analysis of the PELDOR  $V(T)$  gave two broad lines at the distances corresponding to the expected value for the parallel propeller form, whereas the second species has a distance of identical to the antiparallel basket quadruplex, Fig. 7.14a, b and Table 7.3. These conformers are present in a 1:1 ratio in the frozen solution.

The same human telomeric sequence was synthesized and spin-labeled with the more stable TPA **4-18** label [59]. It was injected into the animal hemisphere cytoplasm of stage VI oocytes of *X. laevis* where nucleus-like conditions prevail [60]. For the distance measurements, the telomeric sequence again was labeled in the trinucleotide loop region at the positions 5 and 11 [55, 59]. And again, two distances were found from analysis of  $V(T)$  using a Gaussian line shape, Table 7.3. One distance of 2.9 nm corresponds to the antiparallel basket quadruplex, the second distance of 2.0 nm to the parallel propeller form.

Evidence for a 3 + 1 conformation of a G-quadruplex was obtained in later work [61]. In contrast to previous studies [55, 59], the spin labeled quadruplex was embedded in a long stretch of human telomeric DNA  $d[\text{A}(\text{G}_3\text{T}_2\text{A})_{11}\text{G}_3]$  containing three quadruplex units. The DNA was labeled by TEMPO **4-19** attached at positions 29 and 35 of the DNA sequence. In the presence of  $\text{Na}^+$  ions, the distance between the two nitroxyl spin labels in the middle quadruplex unit of this long DNA was  $r = 3.0 \pm 0.1$  nm which corresponds to the antiparallel basket

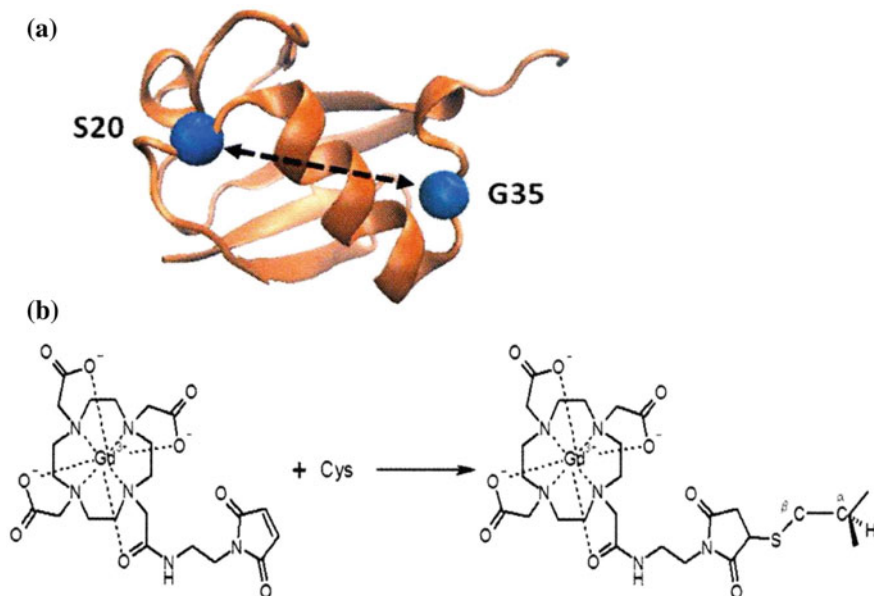


**Fig. 7.15** **a** Ribbon structure of the ubiquitin (PDB 1UBQ), Ser20 and Gly35 were substituted with cysteines and labeled with Gd(III)-DOTA-Maleimide; **b** the labeling reaction. Reprinted from Martorana et al. [62] with permission of American Physical Society, copyrights 2014

quadruplex topology. However in  $K^+$  solution,  $r = 2.5 \pm 0.1$  nm, corresponding to the (3 + 1) hybrid topology, Fig. 7.14c. These results show that PELDOR should prove very useful in further investigations of quadruplex structures and interactions in complex mixtures and even complex cellular systems.

#### 7.4.4 Ubiquitin and Gd(III)

An innovative approach for PELDOR in-cell investigations features: (1) novel Gd(III)-based spin labels and protein linkers that are stable under in-cell conditions; (2) high-field measurements that feature high sensitivity with Gd(III), thus allowing the detection of low concentrations and use of small sample sizes; (3) efficient delivery of the labeled protein into cells by hypo-osmotic shock, reaching in-cell concentrations sufficient for PELDOR measurements while maintaining cell viability; and (4)  $D_2O$  exchange to slow echo decays [62, 63].

These advantages were demonstrated on doubly-labeled ubiquitin in HeLa cells. A mutant of human ubiquitin with two cysteines replacing Ser20 and Gly35, Fig. 7.15a, was doubly labeled with Gd(III)-DOTA maleimide 4-25 [64], Fig. 7.15b, and introduced into HeLa cells by osmotic shock [65, 66]. Operational simplicity, time efficiency, and high probability of cellular viability are attractive

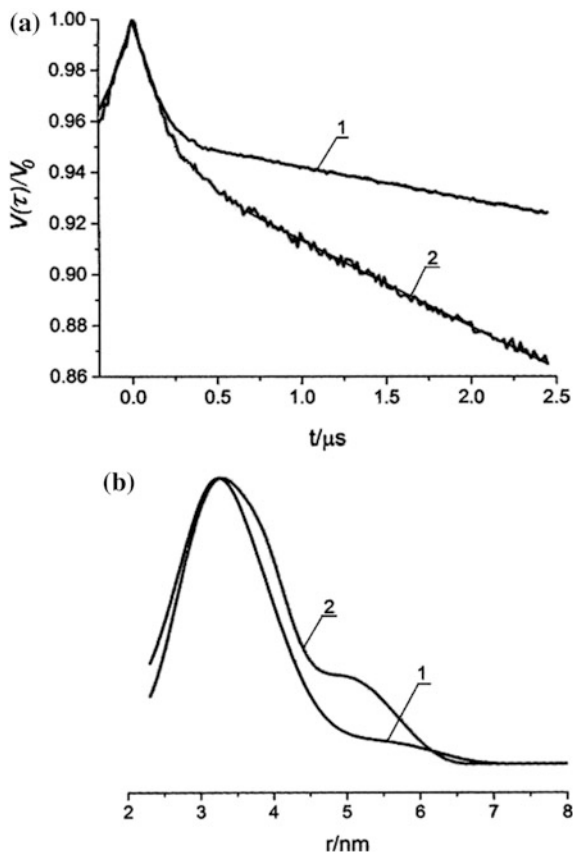


advantages of this technique [62]. Partial deuteration of the intracellular medium by <20% D<sub>2</sub>O was used to slow phase relaxation.

The 4pPELDOR data and analysis are shown in Fig. 7.16. The distance distribution obtained from both *in vitro* and *in-cell* samples is similar: it has a maximum around 3.2 nm and a width of about 1.5 nm. This interspin distance distribution is in good agreement with previous *in vitro* X-band PELDOR measurements on S20C/G35C labeled with conventional nitroxyl spin labels [49, 67]. No comments were made about the right-hand shoulder in  $F(r)$  *in-cell*.

Significant differences were observed in the background  $V(t)$ , which is substantially stronger *in-cell* than in buffer and indicates a higher local concentration *in-cell* of 110  $\mu\text{M}$ . This value exceeds considerably the bulk concentration of 4.5  $\mu\text{M}$  and is larger than that used with hypo-osmotic shock, 100  $\mu\text{M}$ , suggesting localization and inhomogeneous distribution in the cell, in agreement with the fluorescence measurements [62]. The physiological relevance of such localized proteins needs to be carefully considered.

**Fig. 7.16** W-band PELDOR results of doubly-labeled ubiquitin *in vitro* and *in-cell*: **a** experimental DEER trace and background fit: 1 *in vitro* at 25  $\mu\text{M}$ , and 2 *in-cell*; **b** distance distribution  $F(r)$  obtained using Tikhonov regularization for 1 *in vitro*, and 2 *in-cell*. Reprinted from Martorana et al. [62] with permission of American Physical Society, copyright 2014



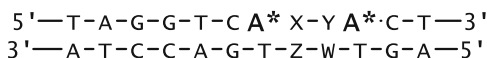
Nevertheless, studies to date in cells and complex systems show that measurements of biomolecule structure and organization by PELDOR has a promising future in biology.

## 7.5 DNA Lesions

The effect of various lesions on DNA structure, in particular, the changes in the distances between spin labels, was studied by PELDOR [68–70]. Lesions in DNA are caused by many factors, such as chemical modification of the DNA at a certain location, nucleotide substitution, nicks in one of the DNA strands in the duplex, etc. All these lesions that chemically modify DNA can cause mutations or cell death. The physical consequences of these lesion on structure and flexibility of the DNA are of particular relevance for understanding the biological effects of these lesions and how they are recognized and repaired.

### 7.5.1 Base Mismatch

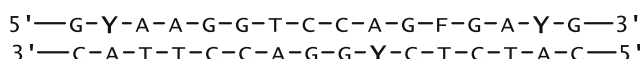
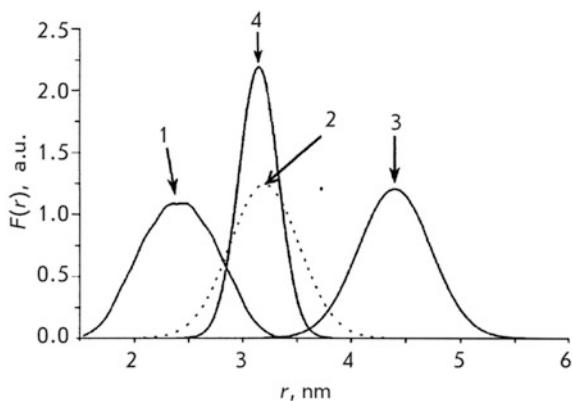
Duplexes containing AA and TT mismatches, i.e., non-canonical pairs, were studied by attaching two TEMPO 4-19 spin labels onto nucleotides on each side of the mismatch [71]:



where A\* is 7-deazaadenosine containing the TEMPO spin label at C7; X-Y is the noncanonical pair dA-dA or dT-dT at positions 8 or 9 of the duplex. The distance between the spins in the canonical duplex, when XY/ZW = AT/TA, was  $r = 1.83$  nm. The distance for the duplexes TT/TA and AT/AA containing the TT or AA noncanonical pair at position 8 was  $r = 1.73$  nm. However,  $r = 1.87$  and 2.08 nm if the duplexes contained noncanonical pairs (AT/TT and AA/TA, respectively) at position 9. Thus, the introduction of a noncanonical pair into position 8 reduces the interspin distance, while the introduction into position 9 increases it as compared to the canonical duplex. The DNA mismatch alters the structure of the adjacent base pairs, but in different way: causing compression or expansion in the two cases examined here.

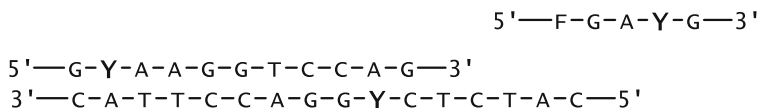
DNA duplexes containing three TEMPO spin labels were also studied [72]. These Y labels were attached to the C5 atom of uridine residues of an alkynyl-oligonucleotide using “click chemistry”. A tetrahydrofuran lesion F was introduced into one of the DNA strands in addition to the spin labels. So, each DNA duplex contained three spin labels and one damaged site.

**Fig. 7.17**  $F(r)$  for a triply-labeled DNA duplex (1, 2, 3) and after treatment with *Endo IV* (4), changes are attributed to double-labeled DNA. Reprinted from Flaender et al. [72] with permission of Wiley and Sons, copyright 2007



The PELDOR  $V(T)$  in this 3-spin system were analyzed using the conventional procedure [73], modified for a 3-spin system [74]. As expected,  $F(r)$  for this system consisted of three lines with peaks at  $r = 2.50$ ,  $3.15$ , and  $4.60$  nm and the widths of  $0.05$ ,  $0.45$ , and  $0.75$  nm, respectively, Fig. 7.17.

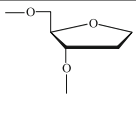
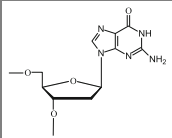
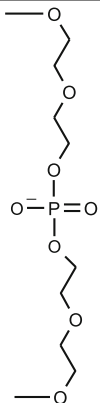
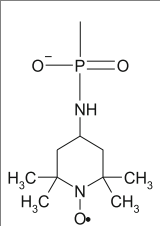
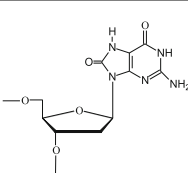
The interaction between this DNA duplex and apurinic/apyrimidinic AP endonuclease IV (*EndoIV*) from *Escherichia coli* was also investigated [72]. *EndoIV* cleaves the damaged strand [75] at the AP site and at AP site analogs containing F residues from damaged deoxyribose. The duplex spin-labeled DNA was cut at the F residue, yielding a duplex containing only two spin labels and a short fragment with one label and the F

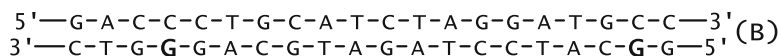
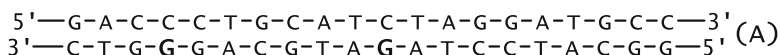


A single line was detected in  $F(r)$  after treatment with *EndoIV*, Fig. 7.17, with  $r = 3.20$  nm and a width of  $0.75$  nm, which was attributed to the spin-labeled duplex that remained after cleavage of the damaged strand. The results obtained demonstrate the potential for using PELDOR in the investigation of 3-spin DNA systems and, more importantly, expand the range of systems that can possibly be used to probe the interaction of DNA with proteins and enzymes.

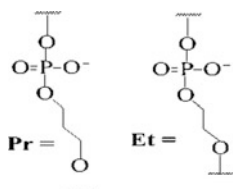
Changes in the inter-label distances in DNA duplexes containing other structural defects and insertions in one of the duplex strands has also been studied [68]. The 20-bp DNA

**Table 7.4** Structures of radical R, nucleotides, and non-nucleotide insertions [69, 70]

				
<b>THF (F)</b>	<b>G</b>	<b>deg2p</b>	<b>R</b>	<b>8oxoG</b>



with TEMPO spin labels attached to guanine residues of one strand at positions (4;11) (**A**) and (4;19) (**B**); the second strand of the duplex contained various lesions—nicks, gaps, modified nucleotides, and bulges, Table 7.4. Two of the non-nucleotide insertions (**Pr**, **Et**) are:



4pPELDOR at 60 or 70 K was used with conventional data analysis methods in each case. The samples contained 50 or 100  $\mu\text{M}$  of spin-labeled DNA in saline with 15–20% glycerol. The  $F(r)$  for the duplex **A** (4;11), undamaged and with various lesions, show a variety of changes, Fig. 7.18. In order to eliminate the orientation selectivity, the PELDOR  $V(T)$  was averaged over 10 measurements by variation of the magnetic field across the EPR spectrum. These measures allow one to reliably assess the error in determining the average distance and the width of lines in the distance spectrum with an error  $\sim 10\%$  [68].

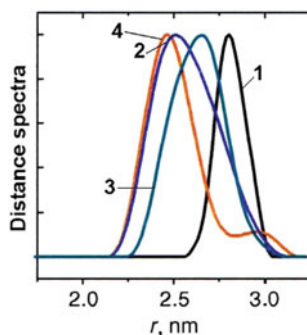


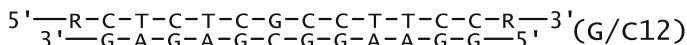
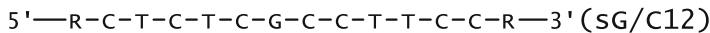
**Fig. 7.18**  $F(r)$  for undamaged DNA **A** / with labels in positions 4 and 11, and the changes when lesions **2 Pr**, **3 Et**, and **4 F** are introduced in the DNA. Reproduced from Sicoli et al. [68] with permission of Oxford University Press, copyrights 2009

The results obtained for the duplexes labeled at positions (4;11) fall into two groups [68]. The first group contained structural lesions **F**, **Pr**, and **Et** at position 7 of the second strand. A significant decrease, from  $r = 2.81$  nm in undamaged **A** to 2.48 nm for **Pr**, along with a broadening of the  $F(r)$  peak from 0.21 to 0.46 nm with the appearance of some asymmetry, was found in this group. A similar situation was observed for duplex **B** labeled at positions (4;19), where the distances changed from  $r = 5.21 \pm 0.04$  nm for the undamaged structure to  $5.02 \pm 0.03$  nm for the damaged duplexes. The width of the distribution function for duplex **B** changed from  $0.33 \pm 0.02$  to  $0.44 \pm 0.05$  nm. In the second group of lesions, **8oxoG**, nick, gap, and bulge, the distance changes were insignificant and due mostly to measurement errors.

When discussing the results, it is usually assumed that the width of the  $F(r)$  peak characterizes the conformational flexibility of the duplex while changes in peak position reflect conformational changes. MD calculations [68] also concluded that the significant changes in  $r$  in the first group of damaged duplexes could be attributed to local changes in the conformations at lesions sites and in the complementary nucleotide of the duplex.

In general, the changes in the damaged DNA in a number of cases [68] are in qualitative agreement with the data obtained by methods such as NMR. The combination of pulse EPR spectroscopy with MD techniques for spin labeled DNA is complementary to conventional methods, such as NMR, CD, FRET, and X-ray crystallography, and provides additional information about DNA lesions and the weak interactions of DNA with other molecules and complexes.

The sensitivity of PELDOR parameters to changes in nucleic acid structure became considerably greater when the spin labels were attached at the termini of relatively short oligonucleotides and their duplexes [69, 70]. Synthetic 12-bp oligonucleotides and their duplexes contained TEMPO **4-19** labels on their 5'- and 3'-terminal phosphate groups:



The G nucleotide located in the center of the G duplex was modified by various insertions and substitutions, Table 7.4.

The spin-labeled DNA was studied in frozen, glassy water/glycerol solutions at 77 K. The  $F(r)$  were determined from the experimental background-free  $V(T)$  using Tikhonov regularization with the use of both the standard algorithm and the Gaussian approximation. The  $F(r)$ , Fig. 7.19a and Table 7.5, demonstrate a 2- to 3-fold narrowing for duplex DNA compared to single-stranded DNA. The insertion of nucleotide analogues results in a reduction in the average interspin distance in the duplexes. In case of the **deg2p** insertion, a noticeable broadening in  $F(r)$  as compared to **G/C12** duplexes was observed. It is obvious that the sharpening in the  $F(r)$  can be attributed to the formation of the DNA double helix, which is characterized by a more rigid structure than single-stranded DNA. The observed width of  $F(r)$  for the undistorted duplex **G/C12** was apparently caused by the random orientation of spin labels due to rotation around the P-N bonds. Considering the fact that the distance between the nitrogen atom and the N-O moiety of the spin label is  $\sim 0.4$  nm, the maximum broadening from the reorientation of spin labels would be 1.6 nm, while the experimental width of  $\Delta = 0.98 \pm 0.1$  nm for the undamaged duplex lies in this range. Effects associated with orientation selection in PELDOR

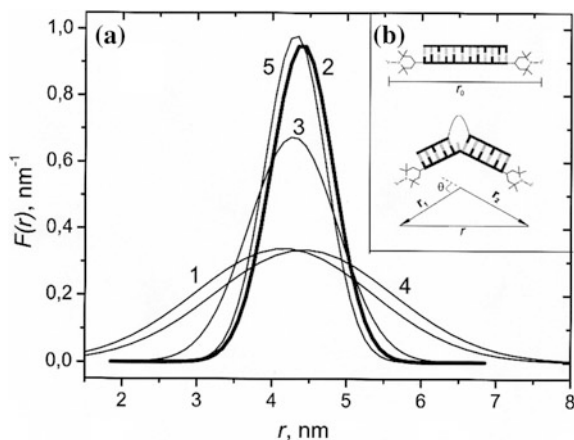


**Fig. 7.19** **a** Gaussian approximation of  $F(r)$  for two spin labels in DNAs: 1 single-stranded oligonucleotide ssG, 2 thick line, duplex dsG, 3: duplex dsG-looped, 4 single-stranded oligonucleotide ssF, 5 duplex dsTHF; **b** schematic representation of spin-labeled DNA *top*: without, and *bottom* with non-nucleotide insert, demonstrating bending and shortening of the distance between labels. Reproduced from Kuznetsov et al. [69] with permission of Royal Society of Chemistry, copyrights 2009

**Table 7.5** Parameters of the distance spectra (nm) for 12-bp oligonucleotides and their DNA duplexes [69]

Sample <sup>a</sup>	Average distance, $r$ , nm	Width $\Delta$ , nm
1. sG/C12	$4.05 \pm 0.05$	$2.8 \pm 0.2$
2. sF/C12	$4.32 \pm 0.05$	$2.85 \pm 0.2$
3. G/C12	$4.35 \pm 0.03$	$0.98 \pm 0.1$
4. deg <sub>2</sub> p/C12	$4.23 \pm 0.03$	$1.39 \pm 0.1$
5. THF/C12	$4.26 \pm 0.03$	$0.95 \pm 0.1$

<sup>a</sup>The symbol s denotes single-stranded DNA

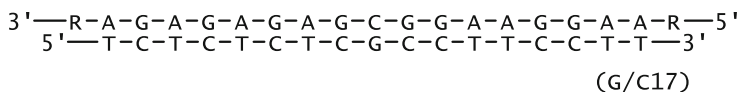
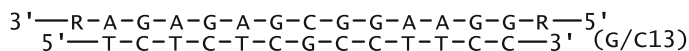
were not observed [68–70], which can also presumably be attributed to the broad, uncorrelated range of spin label orientations.

The introduction of non-nucleotide insertions into the duplex structure affects the average interspin distance. A decrease in the distance raises the possibility of bending of the duplex at the insertion site, due to the additional degree of freedom at the insertion site, Fig. 7.19b. The experimental  $r_0$  in the intact duplex and  $r$  for the distorted duplex can be used to estimate bends with  $\theta = 23^\circ$  in the F/C12 duplex and  $\theta = 27^\circ$  in the looped deg<sub>2</sub>p/C12 duplex.

Any increase in the length and flexibility caused by the insertion in deg<sub>2</sub>p/C12 adds additional broadening in the  $F(r)$ :  $\Delta = 1.39$  nm. The broadening is too large to simply attribute it to the spread in the bending angle of the duplex without taking into account elongation of the duplex. Hence, the bending angle estimated for this insertion is only a lower bound.

Incorporation of a non-nucleotide lesion in a DNA duplex opens the possibility of duplex bending. An increase in the number of bonds in the lesion increases its flexibility. The increase in duplex flexibility near the insertion causes a considerable increase in the range of bending angles and total duplex lengths.

The same approach was used to study lesions in even longer 13-bp and 17-bp DNA duplexes [70]. However, the main aim of the work was to investigate the conformational transformations of DNA during its interaction with the formamidopyrimidine-DNA-glycosylase or Fpg protein from *E. coli*. Fpg is considered to be one of the key factors in the process of DNA repair. The investigated duplexes are:



The structures of the R spin labels, nucleotides, and non-nucleotide insertions are presented in Table 7.4.

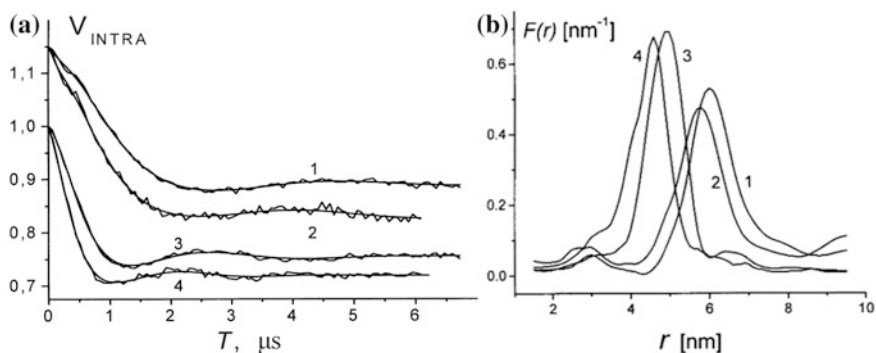


**Fig. 7.20** The  $V_{INTRA}(T)$  for adducted DNA and Fpg. **a** 1 and 2 refer to DNA G/C<sup>17</sup> and THF/C<sup>17</sup>/Fpg, respectively, 3 and 4 refer to DNA G/C<sup>13</sup> and THF/C<sup>13</sup>/Fpg, respectively, 1 and 2 are shifted upwards 0.15, the smooth curves are calculated using the  $F(r)$  **b** the  $F(r)$  between labels neglecting orientation selection, 1 and 2 refer to DNA G/C<sup>17</sup> and THF/C<sup>17</sup>/Fpg, respectively, 3 and 4 refer to DNA G/C<sup>13</sup> and THF/C<sup>13</sup>/Fpg, respectively. Reproduced from Kuznetsov et al. [70] with permission of Royal Society of Chemistry, copyright 2011

**Table 7.6** Parameters (nm) of the distance distribution function  $F(r)$  between two spin labels in the DNA duplexes [70]

Sample	$r_{\max}$ , nm <sup>a</sup>	$\Delta$ , nm <sup>a</sup>
G/C13	4.96	1.12
8-oxoG/C13	4.96	1.15
THF/C13	4.83	1.12
THF/C13/Fpg	4.60	1.2
G/C13/Fpg	4.78	1.1
G/C17	6.00	1.2
8-oxoG/C17	6.02	1.25
THF/C17	5.98	1.23
THF/C17/Fpg	5.76	1.2
G/C17/Fpg	5.99	1.4

<sup>a</sup> $r_{\max}$  and  $\Delta$  were measured with errors of 0.8 and 10%, respectively

The analysis of the  $V(T)$ , Fig. 7.20a, gave the distance distribution  $F(r)$ , Fig. 7.20b, the distance at the peak maximum,  $r_{\max}$  with 0.8% accuracy, and the width of the line at half-height  $\Delta$  with 10% accuracy, Table 7.6.

The positions of the spin labels at the 5'- and 3'-terminal ends of the complementary second oligonucleotide of the DNA duplex made them sensitive to DNA curvature caused by either the damaged sites or the formation of complexes with an enzyme. The Fpg protein from *E. coli* caused bending even in the undamaged 13-bp duplex. A similar result has been obtained from the X-ray structure of Fpg from *Bacillus stearothermophilus* [70, 76, 77]. However, no bend was detected for the undamaged 17-bp duplex in the presence of Fpg. This could be attributed to the fact



that the enzyme occupies a 10-bp DNA segment and cannot move or slide along the short DNA duplex, while sliding is possible during binding to the 17-bp DNA duplex, so Fpg may bind differently to the two undamaged duplexes. It cannot be ruled out, however, that the conformational mobility of the spin labels on the 17-bp duplex is greater than on the 13-bp duplex, which is supported by an increase in the width of  $F(r)$  for the 17-bp duplex, Table 7.6.

In free DNA duplexes containing **8oxoG**, changes in the interspin distances relative to the undamaged duplex have not been seen. This is not surprising, since **8oxoG** hardly changes the DNA structure. Duplexes containing the major cyclic **F** lesion show a considerable reduction in the interspin distance, a result supported by MD computer simulations [70].

During the interaction between the duplexes and Fpg from *E. coli*, bending occurred in both the 13-bp and 17-bp duplexes. This result correlates with the X-ray structures for the cross-linked adduct of Fpg and the AP site [76–78]. It is important to mention that the X-ray data provides information on the damaged DNA region, whereas PELDOR provides complementary information on changes in the global structure.

The bending of the DNA helix near the damaged nucleotide from PELDOR provides new information about the mechanism for recognition of damage by DNA repair enzymes. Detection of the bending allows one to understand why enzymes that slide along the DNA strand would stop at the damaged sites to repair them. The data is also important for understanding other enzymes that search for specific DNA sites.

In our opinion, the data obtained from PELDOR significantly contributes to the investigation of the structure and properties of DNA and RNA. This method opens new perspectives for studying complex nonlinear structures, interactions between polynucleotides and enzymes, proteins, and membranes. The potential of PELDOR as a method for structural studies will undoubtedly increase with the development of pulse EPR spectroscopy.

## References

1. Schiemann O, Prisner TF (2007) Long-range distance determinations in biomacromolecules by EPR spectroscopy. *Q Rev Biophys* 40(1):1–53. <https://doi.org/10.1017/S003358350700460x>
2. Jeschke G, Polyhach Y (2007) Distance measurements on spin-labelled biomacromolecules by pulsed electron paramagnetic resonance. *Phys Chem Chem Phys* 9(16):1895–1910. <https://doi.org/10.1039/B614920k>
3. Tsvetkov YD, Milov AD, Maryasov AG (2008) Pulse electron-electron double resonance (PELDOR) as nanometre range EPR spectroscopy. *Usp Khim* 77(6):515–550
4. Sowa GZ, Qin PZ (2008) Site-directed spin labeling studies on nucleic acid structure and dynamics. *Prog Nucleic Acid Re* 82:147–197. [https://doi.org/10.1016/S0079-6603\(08\)00005-6](https://doi.org/10.1016/S0079-6603(08)00005-6)
5. Schiemann O (2009) Mapping global folds of oligonucleotides by pulsed electron-electron double resonance. *Meth Enzymol* 469: Biophysical, chemical, and functional probes of RNA structure, interactions and folding, *Pt B* 469:329–351. [https://doi.org/10.1016/s0076-6879\(09\)69016-9](https://doi.org/10.1016/s0076-6879(09)69016-9)

6. Reginsson GW, Schiemann O (2011) Studying bimolecular complexes with pulsed electron-electron double resonance spectroscopy. *Biochem Soc T* 39:128–139. <https://doi.org/10.1042/Bst0390128>
7. Reginsson GW, Schiemann O (2011) Pulsed electron-electron double resonance: beyond nanometre distance measurements on biomacromolecules. *Biochem J* 434:353–363. <https://doi.org/10.1042/Bj20101871>
8. Schiemann O, Weber A, Edwards TE, Prisner TF, Sigurdsson ST (2003) Nanometer distance measurements on RNA using PELDOR. *J Am Chem Soc* 125(12):3434–3435
9. Kolhe P, Amend E, Singh SK (2010) Impact of freezing on pH of buffered solutions and consequences for monoclonal antibody aggregation. *Biotechnol Prog* 26(3):727–733. <https://doi.org/10.1002/btpr.377>
10. Ward R, Keeble DJ, El-Mkami H, Norman DG (2007) Distance determination in heterogeneous DNA model systems by pulsed EPR. *ChemBioChem* 8(16):1957–1964. <https://doi.org/10.1002/cbic.200700245>
11. Schiemann O, Piton N, Mu YG, Stock G, Engels JW, Prisner TF (2004) A PELDOR-based nanometer distance ruler for oligonucleotides. *J Am Chem Soc* 126(18):5722–5729. <https://doi.org/10.1021/ja0393877>
12. Piton N, Mu YG, Stock G, Prisner TF, Schiemann O, Engels JW (2007) Base-specific spin-labeling of RNA for structure determination. *Nucleic Acids Res* 35(9):3128–3143
13. Cai Q, Kusnetzow AK, Hubbell WL, Haworth IS, Gacho GPC, Van Eps N, Hideg K, Chambers EJ, Qin PZ (2006) Site-directed spin labeling measurements of nanometer distances in nucleic acids using a sequence-independent nitroxide probe. *Nucleic Acids Res* 34(17):4722–4730. <https://doi.org/10.1093/nar/gkl546>
14. Cai Q, Kusnetzow AK, Hideg K, Price EA, Haworth IS, Qin PZ (2007) Nanometer distance measurements in RNA using site-directed spin Labeling. *Biophys J* 93(6):2110–2117. <https://doi.org/10.1529/biophysj.107.109439>
15. Shevelev GY, Krumkacheva OA, Lomzov AA, Kuzhelev AA, Trukhin DV, Rogozhnikova OY, Tormyshev VM, Pyshnyi DV, Fedin MV, Bagryanskaya EG (2015) Triarylmethyl labels: toward improving the accuracy of EPR nanoscale distance measurements in DNAs. *J Phys Chem B* 119(43):13641–13648
16. Shevelev GY, Krumkacheva OA, Lomzov AA, Kuzhelev AA, Rogozhnikova OY, Trukhin DV, Troitskaya TI, Tormyshev VM, Fedin MV, Pyshnyi DV, Bagryanskaya EG (2014) Physiological-temperature distance measurement in nucleic acid using triarylmethyl-based spin labels and pulsed dipolar EPR spectroscopy. *J Am Chem Soc* 136(28):9874–9877. <https://doi.org/10.1021/ja505122n>
17. Raitsimring AM, Gunanathan C, Potapov A, Efremenko I, Martin JML, Milstein D, Goldfarb D (2007) Gd<sup>3+</sup> complexes as potential spin labels for high field pulsed EPR distance measurements. *J Am Chem Soc* 129(46):14138–14139. <https://doi.org/10.1021/ja075544g>
18. Potapov A, Song Y, Meade TJ, Goldfarb D, Astashkin AV, Raitsimring A (2010) Distance measurements in model bis-Gd(III) complexes with flexible “bridge”. Emulation of biological molecules having flexible structure with Gd(III) labels attached. *J Magn Reson* 205 (1):38–49
19. Song Y, Meade TJ, Astashkin AV, Klein EL, Enemark JH, Raitsimring A (2011) Pulsed dipolar spectroscopy distance measurements in biomacromolecules labeled with Gd(III) markers. *J Magn Reson* 210(1):59–68. <https://doi.org/10.1016/j.jmr.2011.02.010>
20. Yang ZY, Kise D, Saxena S (2010) An approach towards the measurement of nanometer range distances based on Cu<sup>2+</sup> Ions and ESR. *J Phys Chem B* 114(18):6165–6174. <https://doi.org/10.1021/jp911637s>
21. Sicoli G, Mathis G, Delalande O, Boulard Y, Gasparutto D, Gambarelli S (2008) Double electron-electron resonance (DEER): a convenient method to probe DNA conformational changes. *Angew Chem Int Edit* 47(4):735–737. <https://doi.org/10.1002/anie.200704133>
22. Yu H, Mu YG, Nordenskiöld L, Stock G (2008) Influence of nitroxide spin labels on RNA structure: a molecular dynamics simulation study. *J Chem Theory Comput* 4(10):1781–1787. <https://doi.org/10.1021/ct800266e>

23. Romainczyk O, Endeward B, Prisner TF, Engels JW (2011) The RNA-DNA hybrid structure determined by EPR, CD and RNase H1. *Mol BioSyst* 7(4):1050–1052. <https://doi.org/10.1039/c0mb00258e>
24. Savitsky A, Dubinskii AA, Flores M, Lubitz W, Mobius K (2007) Orientation-resolving pulsed electron dipolar high-field EPR spectroscopy on disordered solids: I. Structure of spin-correlated radical pairs in bacterial photosynthetic reaction centers. *J Phys Chem B* 111(22):6245–6262. <https://doi.org/10.1021/jp070016c>
25. Marko A, Margraf D, Yu H, Mu Y, Stock G, Prisner T (2009) Molecular orientation studies by pulsed electron-electron double resonance experiments. *J Chem Phys* 130(6):064102. <https://doi.org/10.1063/1.3073040>
26. Marko A, Margraf D, Cekan P, Sigurdsson ST, Schiemann O, Prisner TF (2010) Analytical method to determine the orientation of rigid spin labels in DNA. *Phys Rev E* 81(2):021911. <https://doi.org/10.1103/PhysRevE.81.021911>
27. Schiemann O, Cekan P, Margraf D, Prisner TF, Sigurdsson ST (2009) Relative orientation of rigid nitroxides by PELDOR: beyond distance measurements in nucleic acids. *Angew Chem Int Edit* 48(18):3292–3295
28. Barhate N, Cekan P, Massey AP, Sigurdsson ST (2007) A nucleoside that contains a rigid nitroxide spin label: a fluorophore in disguise. *Angew Chem Int Edit* 46(15):2655–2658
29. Gophane DB, Endeward B, Prisner TF, Sigurdsson ST (2014) Conformationally restricted isoindoline-derived spin labels in duplex DNA: distances and rotational flexibility by pulsed electron-electron double resonance spectroscopy. *Chem-Eur J* 20(48):15913–15919. <https://doi.org/10.1002/chem.201403726>
30. Tkach I, Halbmaier K, Hobartner C, Bennati M (2014) High-frequency 263 GHz PELDOR. *Appl Magn Reson* 45(10):969–979. <https://doi.org/10.1007/s00723-014-0581-z>
31. Hagerman PJ (1988) Flexibility of DNA. *Annu Rev Biophys* 17:265–286
32. Gore J, Bryant Z, Nollmann M, Le MU, Cozzarelli NR, Bustamante C (2006) DNA overwinds when stretched. *Nature* 442(7104):836–839. <https://doi.org/10.1038/nature04974>
33. Marko JF (1997) Stretching must twist DNA. *Europhys Lett* 38(3):183–188. <https://doi.org/10.1209/epl/i1997-00223-5>
34. Mathew-Fenn RS, Das R, Harbury PAB (2008) Remeasuring the double helix. *Science* 322(5900):446–449. <https://doi.org/10.1126/science.1158881>
35. Marko A, Denysenkov V, Margraf D, Cekan P, Schiemann O, Sigurdsson ST, Prisner TF (2011) Conformational flexibility of DNA. *J Am Chem Soc* 133(34):13375–13379
36. Sicoli G, Wachowius F, Bennati M, Hobartner C (2010) Probing secondary structures of spin-labeled RNA by pulsed EPR spectroscopy. *Angew Chem Int Edit* 49(36):6443–6447. <https://doi.org/10.1002/anie.201000713>
37. Krstic I, Frolow O, Sezer D, Endeward B, Weigand JE, Suess B, Engels JW, Prisner TF (2010) PELDOR spectroscopy reveals preorganization of the neomycin-responsive riboswitch tertiary structure. *J Am Chem Soc* 132(5):1454–1455. <https://doi.org/10.1021/ja9077914>
38. Grytz CM, Marko A, Cekan P, Sigurdsson ST, Prisner TF (2016) Flexibility and conformation of the cocaine aptamer studied by PELDOR. *Phys Chem Chem Phys* 18(4):2993–3002. <https://doi.org/10.1039/c5cp06158j>
39. Kim NK, Bowman MK, DeRose VJ (2010) Precise mapping of RNA tertiary structure via nanometer distance measurements with double electron-electron resonance spectroscopy. *J Am Chem Soc* 132(26):8882–8884. <https://doi.org/10.1021/ja101317g>
40. Zhang XJ, Tung CS, Sowa GZ, Hatmal MM, Haworth IS, Qin PZ (2012) Global structure of a three-way junction in a Phi29 packaging RNA dimer determined using site-directed spin labeling. *J Am Chem Soc* 134(5):2644–2652. <https://doi.org/10.1021/ja2093647>
41. Freeman ADJ, Ward R, El Mkami H, Lilley DMJ, Norman DG (2011) Analysis of conformational changes in the DNA junction-resolving enzyme T7 endonuclease I on binding a four-way junction using EPR. *Biochemistry-U S A* 50(46):9963–9972. <https://doi.org/10.1021/bi2011898>

42. Danielsson J, Inomata K, Murayama S, Tochio H, Lang LS, Shirakawa M, Oliveberg M (2013) Pruning the ALS-associated protein SOD1 for in-cell NMR. *J Am Chem Soc* 135 (28):10266–10269. <https://doi.org/10.1021/ja404425r>
43. Banci L, Barbieri L, Bertini I, Luchinat E, Secci E, Zhao YG, Aricescu AR (2013) Atomic-resolution monitoring of protein maturation in live human cells by NMR. *Nat Chem Biol* 9(5):297–300. <https://doi.org/10.1038/Nchembio.1202>
44. Sakai T, Tochio H, Tenno T, Ito Y, Kokubo T, Hiroaki H, Shirakawa M (2006) In-cell NMR spectroscopy of proteins inside *Xenopus laevis* oocytes. *J Biomol NMR* 36(3):179–188. <https://doi.org/10.1007/s10858-006-9079-9>
45. Ogino S, Kubo S, Umemoto R, Huang SX, Nishida N, Shimada I (2009) Observation of NMR signals from proteins introduced into living mammalian cells by reversible membrane permeabilization using a pore-forming toxin, streptolysin O. *J Am Chem Soc* 131(31):10834–10835. <https://doi.org/10.1021/ja904407w>
46. Azarkh M, Singh V, Okle O, Seemann IT, Dietrich DR, Hartig JS, Drescher M (2013) Site-directed spin-labeling of nucleotides and the use of in-cell EPR to determine long-range distances in a biologically relevant environment. *Nat Protoc* 8(1):131–147. <https://doi.org/10.1038/nprot.2012.136>
47. Azarkh M, Okle O, Eyring P, Dietrich DR, Drescher M (2011) Evaluation of spin labels for in-cell EPR by analysis of nitroxide reduction in cell extract of *Xenopus laevis* oocytes. *J Magn Reson* 212(2):450–454. <https://doi.org/10.1016/j.jmr.2011.07.014>
48. Krstic I, Hansel R, Romainczyk O, Engels JW, Dotsch V, Prisner TF (2011) Long-range distance measurements on nucleic acids in cells by pulsed EPR spectroscopy. *Angew Chem Int Edit* 50(22):5070–5074. <https://doi.org/10.1002/anie.201100886>
49. Igarashi R, Sakai T, Hara H, Tenno T, Tanaka T, Tochio H, Shirakawa M (2010) Distance determination in proteins inside *Xenopus laevis* oocytes by double electron-electron resonance experiments. *J Am Chem Soc* 132(24):8228–8229. <https://doi.org/10.1021/ja906104e>
50. Bowman MK, Maryasov AG, Kim N, DeRose VJ (2004) Visualization of distance distribution from pulsed double electron-electron resonance data. *Appl Magn Reson* 26(1–2):23–39. <https://doi.org/10.1007/Bf03166560>
51. Nakata M, Zanchetta G, Chapman BD, Jones CD, Cross JO, Pindak R, Bellini T, Clark NA (2007) End-to-end stacking and liquid crystal condensation of 6-to 20-base pair DNA duplexes. *Science* 318(5854):1276–1279. <https://doi.org/10.1126/science.1143826>
52. Duchardt-Ferner E, Weigand JE, Ohlenschlager O, Schnidtker SR, Suess B, Wohnert J (2010) Highly modular structure and ligand binding by conformational capture in a minimalistic riboswitch. *Angew Chem Int Edit* 49(35):6216–6219. <https://doi.org/10.1002/anie.201001339>
53. Nozinovic S, Furtig B, Jonker HRA, Richter C, Schwalbe H (2010) High-resolution NMR structure of an RNA model system: the 14-mer cUUCGg tetraloop hairpin RNA. *Nucleic Acids Res* 38(2):683–694. <https://doi.org/10.1093/nar/gkp956>
54. Bochman ML, Paeschke K, Zakian VA (2012) DNA secondary structures: stability and function of G-quadruplex structures. *Nat Rev Genet* 13(11):770–780. <https://doi.org/10.1038/nrg3296>
55. Singh V, Azarkh M, Exner TE, Hartig JS, Drescher M (2009) Human telomeric quadruplex conformations studied by pulsed EPR. *Angew Chem Int Edit* 48(51):9728–9730. <https://doi.org/10.1002/anie.200902146>
56. Wang Y, Patel DJ (1993) Solution structure of the human telomeric repeat d[AG<sub>3</sub>(T<sub>2</sub>AG<sub>3</sub>)<sub>3</sub>] G-tetraplex. *Structure* 1(4):263–282. [https://doi.org/10.1016/0969-2126\(93\)90015-9](https://doi.org/10.1016/0969-2126(93)90015-9)
57. Phan AT, Kuryavyi V, Luu KN, Patel DJ (2007) Structure of two intramolecular G-quadruplexes formed by natural human telomere sequences in K<sup>+</sup> solution. *Nucleic Acids Res* 35(19):6517–6525. <https://doi.org/10.1093/nar/gkm706>
58. Parkinson GN, Lee MPH, Neidle S (2002) Crystal structure of parallel quadruplexes from human telomeric DNA. *Nature* 417(6891):876–880. <https://doi.org/10.1038/nature755>

59. Azarkh M, Singh V, Okle O, Dietrich DR, Hartig JS, Drescher M (2012) Intracellular conformations of human telomeric quadruplexes studied by electron paramagnetic resonance spectroscopy. *ChemPhysChem* 13(6):1444–1447. <https://doi.org/10.1002/cphc.201100980>
60. Shiohara K, Tashiro K, Yamana K, Sameshima M (1987) Electron-microscopic studies of giant nucleus-like structure formed by lambda DNA introduced into the cytoplasm of *Xenopus laevis* fertilized-eggs and embryos. *Cell Differ Dev* 20(4):253–261. [https://doi.org/10.1016/0045-6039\(87\)90470-2](https://doi.org/10.1016/0045-6039(87)90470-2)
61. Singh V, Azarkh M, Drescher M, Hartig JS (2012) Conformations of individual quadruplex units studied in the context of extended human telomeric DNA. *Chem Commun* 48(66):8258–8260. <https://doi.org/10.1039/c2cc32012f>
62. Martorana A, Bellapadrona G, Feintuch A, Di Gregorio E, Aime S, Goldfarb D (2014) Probing protein conformation in cells by EPR distance measurements using Gd<sup>3+</sup> spin labeling. *J Am Chem Soc* 136(38):13458–13465. <https://doi.org/10.1021/ja5079392>
63. Goldfarb D (2014) Gd<sup>3+</sup> spin labeling for distance measurements by pulse EPR spectroscopy. *Phys Chem Chem Phys* 16(21):9685–9699. <https://doi.org/10.1039/c3cp53822b>
64. Thonon D, Jacques V, Desreux JF (2007) A gadolinium triacetic monoamide DOTA derivative with a methanethiosulfonate anchor group. Relaxivity properties and conjug. *Contrast Media Mol I* 2(1):24–34. <https://doi.org/10.1002/cmml.121>
65. Rossi L, Serafini S, Pierge F, Antonelli A, Cerasi A, Fraternali A, Chiarantini L, Magnani M (2005) Erythrocyte-based drug delivery. *Expert Opin Drug Deliv* 2(2):311–322. <https://doi.org/10.1517/17425247.2.2.311>
66. Markov DE, Boeve H, Gleich B, Borgert J, Antonelli A, Sfara C, Magnani M (2010) Human erythrocytes as nanoparticle carriers for magnetic particle imaging. *Phys Med Biol* 55(21):6461–6473. <https://doi.org/10.1088/0031-9155/55/21/008>
67. Hara H, Tenno T, Shirakawa M (2007) Distance determination in human ubiquitin by pulsed double electron-electron resonance and double quantum coherence ESR methods. *J Magn Reson* 184(1):78–84. <https://doi.org/10.1016/j.jmr.2006.09.017>
68. Sicoli G, Mathis G, Aci-Seche S, Saint-Pierre C, Boulard Y, Gasparutto D, Gambarelli S (2009) Lesion-induced DNA weak structural changes detected by pulsed EPR spectroscopy combined with site-directed spin labelling. *Nucleic Acids Res* 37(10):3165–3176. <https://doi.org/10.1093/nar/gkp165>
69. Kuznetsov NA, Milov AD, Koval VV, Samoilova RI, Grishin YA, Knorre DG, Tsvetkov YD, Fedorova OS, Dzuba SA (2009) PELDOR study of conformations of double-spin-labeled single- and double-stranded DNA with non-nucleotide inserts. *Phys Chem Chem Phys* 11(31):6826–6832. <https://doi.org/10.1039/b904873a>
70. Kuznetsov NA, Milov AD, Isaev NP, Vorobjev YN, Koval VV, Dzuba SA, Fedorova OS, Tsvetkov YD (2011) PELDOR analysis of enzyme-induced structural changes in damaged DNA duplexes. *Mol BioSyst* 7(9):2670–2680. <https://doi.org/10.1039/c1mb05189j>
71. Wunnicke D, Ding P, Seela F, Steinhoff HJ (2012) Site-directed spin labeling of DNA reveals mismatch-induced nanometer distance changes between flanking nucleotides. *J Phys Chem B* 116(14):4118–4123. <https://doi.org/10.1021/jp212421c>
72. Flaender M, Sicoli G, Aci-Seche S, Reignier T, Maurel V, Saint-Pierre C, Boulard Y, Gambarelli S, Gasparutto D (2011) A triple spin-labeling strategy coupled with DEER analysis to detect DNA modifications and enzymatic repair. *ChemBioChem* 12(17):2560–2563. <https://doi.org/10.1002/cbic.201100550>
73. Jeschke G, Chechik V, Ionita P, Godt A, Zimmermann H, Banham J, Timmel CR, Hilger D, Jung H (2006) DeerAnalysis2006—a comprehensive software package for analyzing pulsed ELDOR data. *Appl Magn Reson* 30(3–4):473–498. <https://doi.org/10.1007/Bf03166213>
74. Jeschke G, Sajid M, Schulte M, Godt A (2009) Three-spin correlations in double electron-electron resonance. *Phys Chem Chem Phys* 11(31):6580–6591
75. Takeuchi M, Lillis R, Demple B, Takeshita M (1994) Interactions of *Escherichia coli* endonuclease-IV and exonuclease-III with abasic sites in DNA. *J Biol Chem* 269(34):21907–21914

76. Banerjee A, Santos WL, Verdine GL (2006) Structure of a DNA glycosylase searching for lesions. *Science* 311(5764):1153–1157. <https://doi.org/10.1126/science.1120288>
77. Qi Y, Spong MC, Nam K, Karplus M, Verdine GL (2010) Entrapment and structure of an extrahelical guanine attempting to enter the active site of a bacterial DNA glycosylase, MutM. *J Biol Chem* 285(2):1468–1478. <https://doi.org/10.1074/jbc.M109.069799>
78. Gilboa R, Zharkov DO, Golan G, Fernandes AS, Gerchman SE, Matz E, Kycia JH, Grollman AP, Shoham G (2002) Structure of formamidopyrimidine-DNA glycosylase covalently complexed to DNA. *J Biol Chem* 277(22):19811–19816. <https://doi.org/10.1074/jbc.M202058200>